Canopy Reflectance, Photosynthesis, and Transpiration. II. The Role of Biophysics in the Linearity of Their Interdependence

P. J. SELLERS

COLAI, Department of Meteorology, University of Maryland, College Park, Maryland 20742

A two-stream approximation model of radiative transfer is used to calculate values of hemispheric canopy reflectance in the visible and near-infrared wavelength intervals. Simple leaf models of photosynthesis and stomatal resistance are integrated over leaf orientation and canopy depth to obtain estimates of canopy photosynthesis and bulk stomatal or canopy resistance. The simple ratio (SR) of the near-infrared and visible canopy reflectances has been found to be a near-linear indicator of the photosynthetically active radiation absorbed by the canopy, APAR, minimum canopy resistance, $1/r_c$, and photosynthetic capacity P_c, but a highly nonlinear and therefore less reliable predictor of leaf area index or biomass (Sellers, 1985). This paper extends previous work and investigates the biophysical processes giving rise to the near-linear dependence of APAR, P_c and $1/r_c$ on SR. It is demonstrated that under normal field conditions, i.e., dark soil, the near-infrared reflectance term controls the variation of SR with leaf area index. As a result of this, near-linearity between SR and APAR, P_c or $1/r_c$ will occur if the leaf scattering coefficient in the near-infrared region, ω_N, satisfies the following equality: $\omega_N = 1 - [G(\mu)/2\mu]^2(1 - \omega_\pi)$, where ω_π is the leaf's effective scattering coefficient for PAR, $G(\mu)$ is the average leaf projection in the direction μ, and μ is the cosine of the zenith angle of the incoming flux. This condition is approximately met in nature. It is shown that a variety of satellite sensor combinations are well configured for the estimation of APAR, P_c and $1/r_c$ by responding to leaf scattering coefficients in bands that conform to the above expression. The relationships between SR and APAR, P_c or $1/r_c$ becomes increasingly nonlinear as the soil reflectivity increases.

Introduction

The past few years have seen a considerable rise in interest in the relationship between the spectral reflectance of the vegetated land surface and biometric or biophysical quantities associated with the vegetation. Many researchers have utilized combinations of spectral radiances observed over vegetated surfaces as indicators of the density, health, or biomass of the vegetation. The most commonly used combination of radiances are known as the simple ratio (SR) and the normalized difference vegetation indexes (ND) (sometimes referred to as just the vegetation index) defined by

$$\mathrm{SR} = \frac{R_N}{R_V}, \tag{1a}$$

$$\mathrm{ND} = \frac{R_N - R_V}{R_N + R_V}, \tag{1b}$$

where

SR = simple ratio,

ND = normalized difference,

R_N, R_V = upwelling radiances in the near-infrared and visible spectral regions, respectively.

Initially, researchers investigated the correlation between the simple ratio or the normalized difference of the reflected near-infrared and visible radiances to green leaf area index and/or biomass (Tucker et al., 1981; Curran, 1980). Later

52 Vanderbilt Ave., New York, NY 10017 0034-4257/87/$3.50

work related the simple ratio or normalized difference to the amount of photosynthetically active radiation (PAR) absorbed by the green canopy (Asrar et al., 1984). Starting with Monteith (1977) and continuing with Goward et al. (1985), Heimann et al. (1986), and Fung et al. (1986), the time integral of the absorbed photosynthetically active radiation (APAR) as estimated from either the simple ratio or the normalized difference has been found to be near-linearly related to net primary production (NPP). In a previous paper, Sellers (1985) approached the subject from a theoretical viewpoint and demonstrated with the aid of simple reflectance, photosynthesis and resistance models that the simple ratio or normalized difference:

i. would provide a non-linear but monotonic indication of green leaf area index and/or biomass, but
ii. appeared to be near-linearly related to the amount of absorbed photosynthetically active radiation (APAR), the area-averaged photosynthetic capacity P_c^*, and the inverse canopy resistance function $1/r_c^*$, at the time of observation. The last two quantities represent the *maximum* gross photosynthetic productivity and *minimum* canopy resistance for given illumination conditions.

Essentially, the work of Sellers (1985) suggested that spectral reflectance data were good indicators of *rates* associated with the vegetation (i.e., photosynthesis, transpiration) but unreliable indicators of the *state* of the vegetation (leaf area index, biomass). As the relationship between the reflectance data and such rates was found to be near-linear, time integrals of the reflectance data, suitably weighted by the amount of incident photosynthetically active radiation, should provide reasonable estimates of gross photosynthetic productivity (GPP) and, by extension, net photosynthetic production (NPP). It is important to note, however, that the relationship becomes non-linear at saturating levels of PAR, i.e., canopy photosynthesis does not increase linearly with increasing incident PAR. This has the effect of "levelling off" the intercepted PAR/canopy photosynthesis relationship, a trend which is apparent in the data of Monteith (personal communication).

The experimental evidence and theoretical work mentioned above indicates that the simple ratio or normalized difference vegetation indexes and the vegetation-dependent quantities APAR, P_c^*, and $1/r_c^*$ are near-linearly related. The paper of Sellers (1985) did not advance any physical or biological reasons why this should be so. The theoretical analyses presented in this paper indicate that the proportionality of the leaf scattering coefficients in the visible and near-infrared wavelength regions is the cause of this phenomenon. This proportionality may be used to formulate criteria for assessing the suitability of satellite sensor systems for estimating biophysical quantities. These criteria are used in the last part of the paper to show that some satellite sensor systems are well configured for the estimation of area-averaged canopy photosynthetic and transpirative properties.

Theoretical Revision

This paper continues the analysis of Sellers (1985) in exploring the links between canopy reflectance, photosynthesis, and transpiration. The main objective of the analysis presented here is to

explain why the reflectance indicators of the simple ratio and normalized difference should be near-linearly related to the surface biophysical properties of canopy PAR absorption, photosynthesis, and bulk stomatal resistance.

Sellers (1985) used three simple models to describe the processes of canopy reflectance, photosynthesis, and resistance: These are briefly reviewed below.

Radiative transfer, and hence reflectance and absorption, was described by the two-stream approximation model discussed by Dickinson (1983) and extended by Sellers (1985). This model describes the scattered diffuse flux above, within and below the canopy as having only two directions: upwards and downwards. This represents a considerable simplification compared to physical reality and the more complex numerical models, for example, the paper of Kimes (1984), where the scattered flux is treated as a vector quantity with an infinite number of possible vectors or scattering directions in nature and a relatively large number in numerical models [74 in the case of the Kimes (1984) model]. However, comparisons between the two-stream model, the Kimes (1984) numerical model, and data have shown that as far as vegetation canopy hemispherical reflectances are concerned, the two-stream model is an adequate description of the scattering and absorption processes (Kimes et al., 1986).

The upward, $I\uparrow$, and downward, $I\downarrow$, diffuse fluxes of radiation within the canopy are described by the following equations for the case of an incident direct flux:

$$-\bar{\mu}\frac{dI\uparrow}{dL}+[1-(1-\beta)\omega]I\uparrow-\omega\beta I\downarrow = \omega\bar{\mu}K\beta_0 e^{-KL}, \quad (2a)$$

$$\bar{\mu}\frac{dI\downarrow}{dL}+[1-(1-\beta)\omega]I\downarrow-\omega\beta I\uparrow = \bar{\omega}\mu K(1-\beta_0)e^{-KL}, \quad (2b)$$

where

$I\uparrow, I\downarrow$ = upward and downward diffuse radiative fluxes, normalized by the incident flux,

μ = cosine of the zenith angle of the incident beam,

K = optical depth of direct beam per unit leaf area

$= G(\mu)/\mu$,

$G(\mu)$ = relative projected area of leaf elements in direction $\cos^{-1}\mu$,

$\bar{\mu}$ = average inverse diffuse optical depth per unit leaf area

$= \int_0^1 [\mu'/G(\mu')]\,d\mu'$,

μ' = direction of scattered flux,

ω = scattering coefficient

$= \alpha + \tau$,

α = leaf element reflectance,

τ = leaf element transmittance,

L = cumulative leaf area index,

β, β_0 = upscatter parameters for diffuse and direct beams, respectively.

In (2), the individual phytoelements are treated as isotropic scatterers. Strictly speaking, this is not the case, but the use of this assumption does not seem to be responsible for serious errors.

Physical processes can be attributed to each of the four terms in (2). Equation

(2a) describes the vertical profile of the upward diffuse radiative flux, $I\uparrow$, within the canopy. (It should be noted that both the upward and downward diffuse fluxes are assumed to be completely isotropic.) The first term in (2a) describes the attenuation of the upward diffuse flux as a function of the other three terms. The second term defines that fraction of $I\uparrow$ that is rescattered in an upward direction following interaction with leaf elements. The third term refers to the fraction of the downward diffuse flux $I\downarrow$, which is converted into upward diffuse flux by backscattering. The last term, on the right-hand side of (2a), refers to the contribution to the upward diffuse flux by the scattering of direct incident flux penetrating to the specified depth L in the canopy. Corresponding descriptions may be assigned to the four terms in (2b) which describes the profile of the downward diffuse flux.

The derivation of the values of the parameters $\bar{\mu}$, β, and β_0 is described in Dickinson (1983) and Sellers (1985). Essentially, they are found to be functions of the leaf optical properties, τ and α, and the leaf angle distribution function $O(\xi,\theta)$, where ξ is leaf azimuth angle and θ is the angle of the leaf normal to the local vertical.

Equation (2) may be solved quite simply for the case of an isotropically reflecting soil underlying the vegetation canopy. The appropriate boundary conditions are then:

$$I\downarrow = 0, \qquad L = 0, \tag{3a}$$

$$I\uparrow = \rho_s\left(I\downarrow + e^{-KL_T}\right), \qquad L = L_T, \tag{3b}$$

where

ρ_s = soil reflectance,

L_T = total leaf area index.

The first boundary condition states that all of the incoming flux above the canopy is contributed by direct beam radiation. The second boundary condition simply states that the downcoming radiation at the soil surface, $I\downarrow + e^{-KL_T}$, is reflected isotropically to generate the upward diffuse flux beneath the canopy.

The solution of (2) with (3) yields

$$I\uparrow = \frac{h_1}{\sigma}e^{-KL} + h_2e^{-hL} + h_3e^{hL}, \tag{4a}$$

$$I\downarrow = \frac{h_4}{\sigma}e^{-KL} + h_5e^{-hL} + h_6e^{hL}. \tag{4b}$$

The values of the constants σ, h, and h_1–h_6 are determined from manipulation of (2) and are provided in the Appendix of Sellers (1985).

The canopy hemispherical reflectance for this case is then simply given by

$$a(\mu) = I\uparrow(0) = h_1/\sigma + h_2 + h_3. \tag{5}$$

Suitable boundary conditions may be used in place of (3) and the direct radiation terms on the right-hand sides of (2) dropped from the basic equation set to solve for incident diffuse radiative fluxes (Sellers, 1985).

Of particular importance to the following discussion are the power terms in (4), that is, K and h. K is given by the mean projected area of the leaf elements in the direction of the incident flux, divided by the cosine of that direction, i.e., $G(\mu)/\mu$. The diffuse attenuation term h is obtained from the solution of (2):

$$h = (1/\bar{\mu})[(1-\omega+2\beta\omega)(1-\omega)]^{1/2}. \tag{6}$$

The average inverse diffuse optical depth per unit leaf area, $\bar{\mu}$, is equal to unity for canopies with horizontal or spherically distributed leaves, and is close to unity for most other leaf angle distributions.

In the case of horizontal leaves, or when $\tau = \alpha$, (6) simplifies to

$$h = (1 - \omega)^{1/2}. \tag{7}$$

Sellers (1985) and Kimes et al. (1986) have presented results which compare the predictions of the two-stream model with field data. For illustrative purposes, Fig. 1 shows the variation of surface reflectance in the visible, a_V, and near-infrared, a_N, wavelength intervals as a function of leaf area index and soil reflectance. In these and subsequent figures, the worked examples make use of the vegetation properties listed in Table 1. Two leaf angle distributions are considered: horizontal and spherical. (The latter case, which is a fair approximation for much natural vegetation, is equivalent to the leaves having an angular distribution function like the surface facets of a sphere—it is often referred to as a random distribution.) The

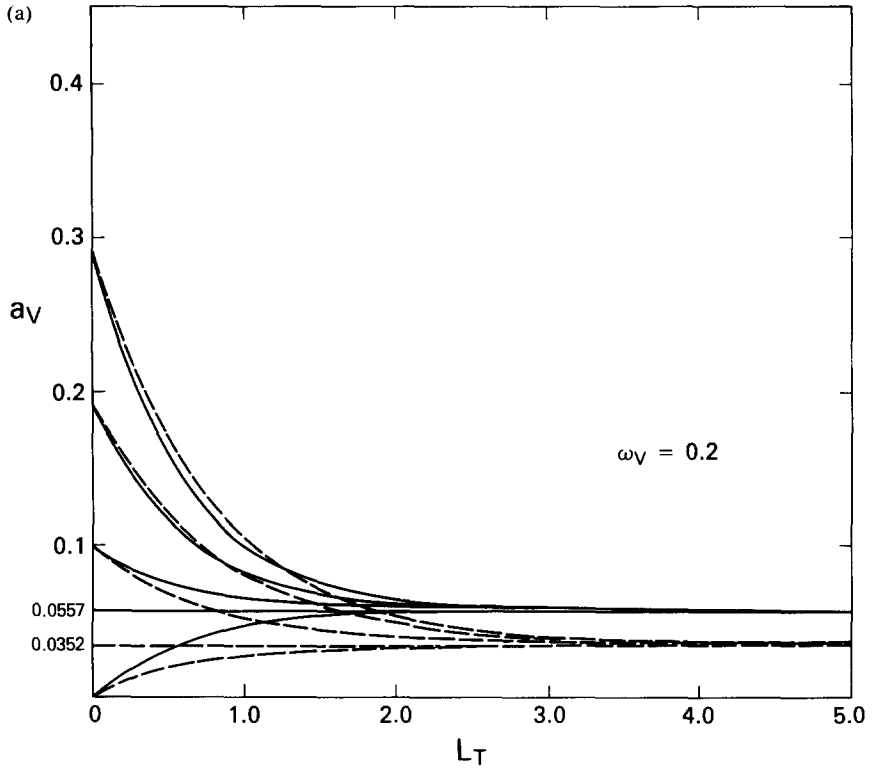

FIGURE 1. Surface hemispherical reflectance as a function of total leaf area index L_T, leaf scattering coefficient ω, and soil reflectance ρ_s. In all cases, solid lines refer to canopies with horizontal leaves, and dashed lines to canopies with spherically distributed leaves. The start point of each line on the vertical (reflectance) axis indicates the background soil reflectance. (a) Reflectances in the visible region; $\omega_V = 0.2$; (b) reflectances in the near-infrared region $\omega_N = 0.8$; (c) reflectances in the near-infrared region, $\omega_N = 0.95$. The horizontal lines on each figure refer to the asymptotic (semiinfinite) canopy reflectance.

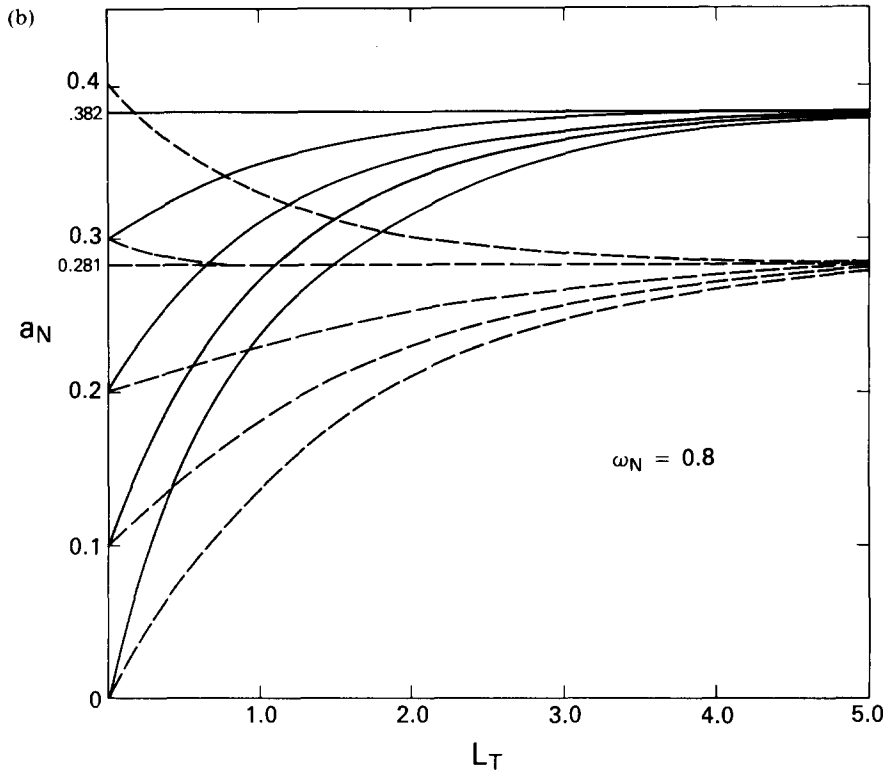
(b)
0.4
.382
0.3
0.281
a_N
0.2
0.1
0
1.0
2.0
3.0
4.0
5.0
L_T
ω_N = 0.8

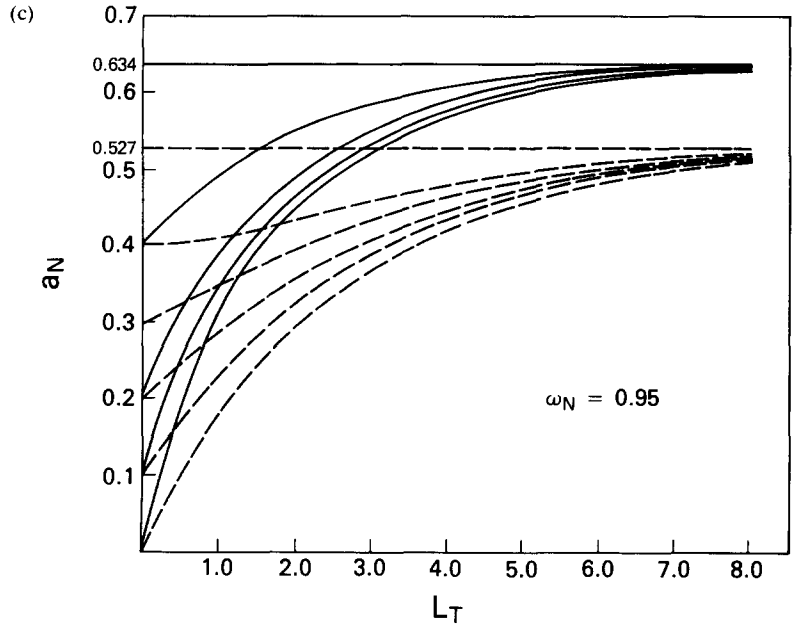
(c)
0.7
0.634
0.6
0.527
0.5
a_N
0.4
0.3
0.2
0.1
1.0
2.0
3.0
4.0
5.0
6.0
7.0
8.0
L_T
ω_N = 0.95

TABLE 1 Optical and Physiological Properties Used for Model Canopy[a]

Leaf Angle Distribution	Horizontal, Spherical
Visible, PAR scattering coefficients ω_V, ω_π	0.2
Near infrared scattering coefficient ω_N	0.8, 0.95
Leaf photosynthesis constants	
a_1 (mg CO_2 dm^{-1} h^{-1})	82.6
b_1 (W m^{-2})	278.4
Leaf stomatal resistance constants	
a_2 (J m^{-3})	8750.0
b_2 (W m^{-2})	6.0
c_2 (s m^{-1})	55.0

[a] The values of $\omega_V = 0.2$ and $\omega_N = 0.8$ may be compared with equivalent values of 0.175 and 0.825, respectively, reported by Dickinson (1983) for the wavelength intervals 0.4–0.7 μm (visible) and 0.7–0.3 μm (near-infrared), respectively. Values of a_1 and b_1 were obtained from curve fits to data of Hesketh and Baker (1967); a_2, b_2, and c_2 from data of Turner (1974), for maize leaves.

leaf scattering coefficient in the visible region, ω_V, is taken as 0.2. Two leaf scattering coefficients are considered in the near-infrared region, $\omega_N = 0.8$ (representative of green leaves in the 1.6–1.8 μm interval) and $\omega_N = 0.95$ (representative of green leaves in the 0.7–1.1 μm interval). The reason for considering two values of ω_N will become apparent in the discussion. In all cases, it is assumed that $\tau = \alpha$, so that (7) holds true. It is also assumed, rather less realistically, that the soil reflectance ρ_s is the same in all spectral regions. (Normally, ρ_s increases gradually with wavelength, a small complication which has been neglected to keep this analysis simple.) Additionally, the incoming radiative fluxes are assumed to be all vertical beams, close to conditions representative of a clear day with a near-overhead sun, i.e., good remote-sensing weather.

Under normal field conditions, when the soil is relatively dark ($\rho_s < 0.1$), we see that the visible reflectance a_V does not vary much with increasing leaf area index, mainly because the rescattering of light in this wavelength interval is so small ($\omega_V = 0.2$). By contrast, the near-infrared canopy reflectance a_N continues to show significant change with increasing leaf area index due to the relatively high scattering coefficient of green leaves ($\omega_N = 0.8$ or 0.95) in this spectral region, see Figure 1.

Because of this, we expect the reflectance indicators SR and ND to be mainly functional on the near-infrared surface reflectance a_N. Figure 2 shows the variation of SR and ND with total leaf area index L_T. Reference to Fig. 1 and a comparison of the absolute values of a_N and a_V will confirm that, for low values of ρ_s, the SR and ND are dominated by the a_N term.

The proportion of PAR absorbed by the vegetation canopy, APAR, may be calculated by

$$\text{APAR} = 1 - a_\pi - (1 - \rho_{s\pi}) \times \left(e^{-K_\pi L_T} + I\downarrow_{(L)}\right), \quad (8)$$

where the subscript π refers to the PAR wavelength interval.

Clearly, derivation of a value for the PAR surface reflectance, a_π, requires the specification of a value of ω_π, the mean leaf scattering coefficient for the effectively used PAR.

The calculation of ω_π is set out later in the paper; it is simply an estimate of the mean leaf scattering coefficient for the PAR wavelength interval with some weighting for the spectral dependences of the solar flux and the photosynthetic ac-

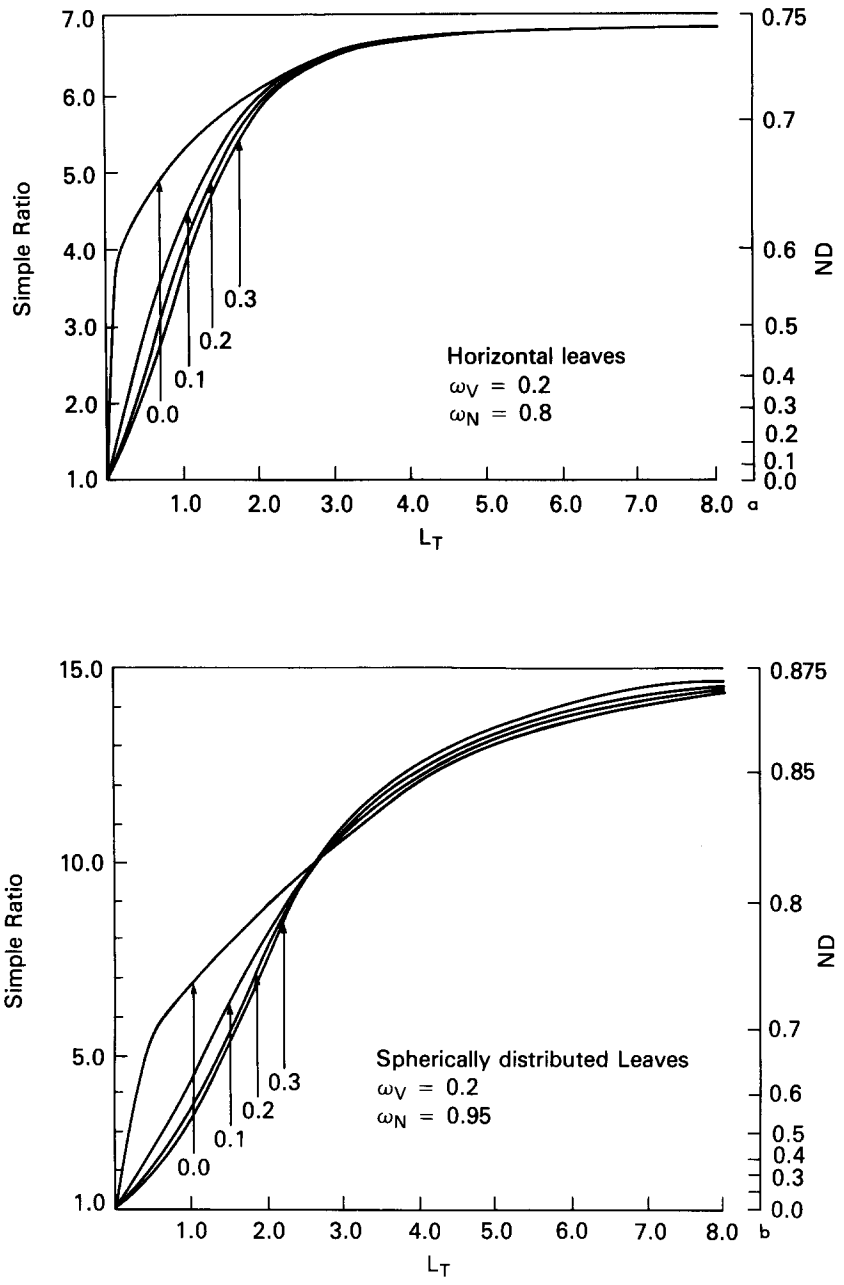

FIGURE 2. Simple ratio (SR) as a function of total leaf area index L_T and soil reflectance ρ_s. (a) Simple ratio calculated for a canopy of horizontal leaves, $\omega_V = 0.2$, $\omega_N = 0.8$. (b) Simple ratio calculated for a canopy of spherically distributed leaves, $\omega_V = 0.2$, $\omega_N = 0.95$. Values of background soil reflectance are marked against each line and are assumed to be constant over the spectrum. Equivalent ND values are shown on the right-hand vertical axes of each figure.

tion efficiency of the leaf. From data, ω_π is calculated to be 0.207 (see later section): here it is taken to be equal to the specified value of ω_V (= 0.2) for the time being. For the bulk of the analysis, therefore, the subscripts V and π are interchangeable. The second term of the left-hand side refers to the proportion of PAR reflected by the surface while the third term refers to the proportion of PAR absorbed by the soil. Figure 3 shows the variation of APAR with total leaf area index L_T.

Canopy photosynthesis and resistance are described by extensions of simple leaf photosynthesis and resistance models, as described in Sellers (1985):

Leaf photosynthesis:

$$P = \left[\frac{a_1 F\downarrow}{b_1 + F\downarrow} - R_d\right] f(\psi_l)\cdot f(T_c)\cdot f(\delta e), \quad (9)$$

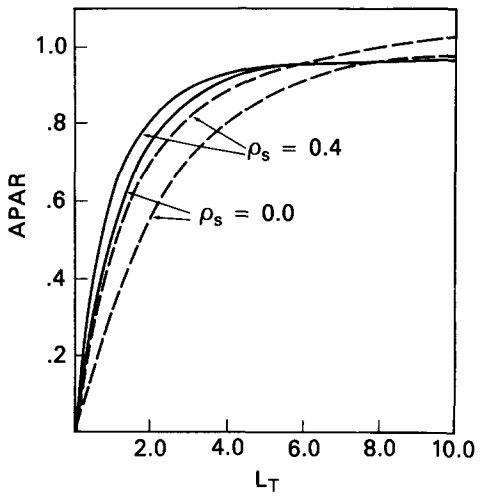

FIGURE 3. Variation of the absorbed fraction of photosynthetically active radiation (APAR) with leaf area index. It is assumed that $\omega_\pi = \omega_V = 0.2$ is representative for the PAR region. Horizontal and spherical leaf angle distributions are indicated by solid and dashed lines respectively; background soil reflectances are marked against the curves.

where

P = leaf photosynthetic rate $(\text{mg CO}_2\,\text{dm}^{-1}\,\text{h}^{-1})$,

$F\downarrow$ = normal (relative to leaf) flux density of incident PAR (W m^{-2}),

R_d = dark respiration rate $(\text{mg CO}_2\,\text{dm}^{-1}\,\text{h}^{-1})$,

a_1, b_1 = constants $(\text{mg CO}_2\,\text{dm}^{-1}\,\text{h}^{-1}, \text{W m}^{-2})$.

Leaf stomatal resistance:

$$r_s = \left(\frac{a_2}{b_2 + F\downarrow} + c_2\right) \cdot [f(\psi_l)\cdot f(T_c)\cdot f(e_a)]^{-1}, \quad (10)$$

where

r_s = leaf stomatal resistance (s m^{-1}),

a_2, b_2, c_2 = constants determined from data or from a_1, b_1, and R_d $(\text{J m}^{-3}, \text{W m}^{-2}, \text{s m}^{-1})$,

$f(\psi_l), f(T_c), f(\delta e)$ = adjustment factors for the effects of leaf water potential ψ_l, temperature T_c, and vapor pressure deficit δe

The dark respiration term R_d in (9) has been dropped from the ensuing analysis partly because there is some controversy about how to specify its variation with increasing leaf area index. R_d is assumed to be a fairly small proportion of P for reasonable values of leaf area index (< 6).

The adjustment factors $f(\psi_l)$, $f(T_c)$, and $f(\delta e)$ are equal to unity under optimal conditions and zero when photosynthesis and transpiration are reduced by adverse environmental conditions; i.e., limiting soil moisture, extremes of temperature, or an excessive vapor pressure deficit, respectively. It is assumed in all the following discussion that light is the only limiting factor, so that $f(\psi_l) = f(T_c) = f(\delta e) = 1$.

The quantities a_1, b_1, a_2, b_2, and c_2 are largely species dependent. If one accepts the arguments favoring a constant ratio between P and the transpiration rate (see Farquhar and von Caemmerer, 1982; Farquhar and Sharkey, 1982), it is relatively easy to derive values of a_2, b_2, and c_2 from a consideration of the photosynthetic equation, (9), and the constant of water use efficiency, and an assumed climatic mean evaporative demand. For the present, however, the values of the constants in (9) and (10) are determined from fitting to data for maize leaves as given in Table 1.

Equations (9) and (10) are taken as good for processes associated with a single leaf exposed to a normal incident PAR flux, $F\downarrow$. In order to obtain the area-averaged canopy photosynthetic rate P_c and resistance r_c, we must integrate (9) and (10) over the depth of the canopy, while taking into account the fact that the leaves may have a range of orientations and therefore a range of projections relative to the incoming flux.

To start with, we assume that PAR is attenuated on its passage down through the canopy according to the Goudriaan (1977) semiempirical expression,

$$F_L = F_0 e^{-kL},$$

where

$$k = [G(\mu)/\mu](1-\omega_\pi)^{1/2}, \qquad (11)$$

F_L, F_0 = PAR fluxes below a leaf area index L and at the top of the canopy, respectively ($\mathrm{W\,m^{-2}}$),

ω_π = effective scattering coefficient for PAR

$\simeq \omega_V$.

Then, with information concerning the leaf angle distribution as given by the leaf angle distribution function $O(\xi, \theta)$, we may combine (9) and (10) with (11) to give the canopy photosynthetic rate and resistance:

$$P_c = \int_0^{L_T}\int_0^{\pi/2}\int_0^{2\pi} P(F,\xi,\theta)O(\xi,\theta) \times \sin\theta\, d\xi\, d\theta\, dL, \qquad (12)$$

$$\frac{1}{r_c} = \int_0^{L_T}\int_0^{\pi/2}\int_0^{2\pi} \frac{O(\xi,\theta)}{r_s(F,\xi,\theta)} \times \sin\theta\, d\xi\, d\theta\, dL. \qquad (13)$$

The leaf angle distribution function is discussed in some detail in Ross (1975)—basically it describes the range of leaf azimuth ξ and inclination θ angles for a given canopy. Its properties are specified such that

$$\int_0^{\pi/2}\int_0^{2\pi} O(\xi,\theta)\sin\theta\, d\xi\, d\theta = 1. \qquad (14)$$

Solutions to (12) and (13) for a range of canopy types are reproduced in Sellers (1985). Figures 4 and 5 show how P_c and $1/r_c$ vary with leaf area index and incident PAR flux density for the leaf proper-

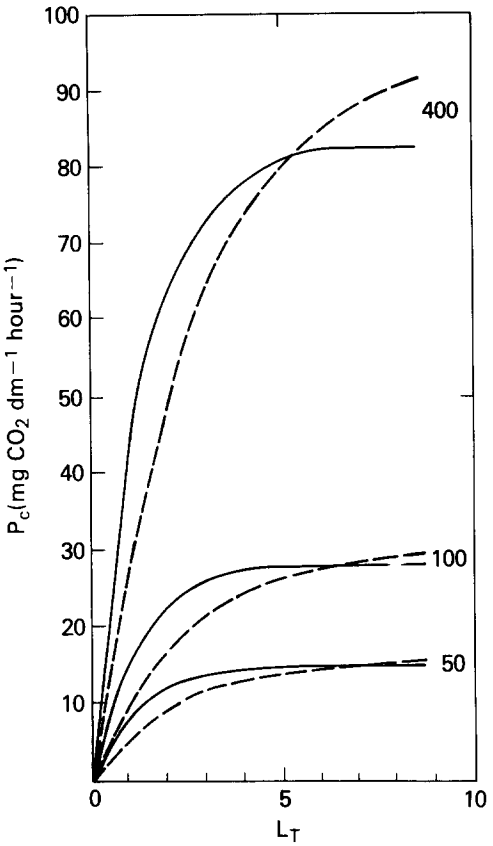

FIGURE 4. Canopy photosynthesis P_c, as a function of leaf area index L_T, PAR flux density (marked against the curves in W m^{-2}), and leaf angle distributions (solid lines for horizontal leaves; dashed lines for spherical leaf angle distributions).

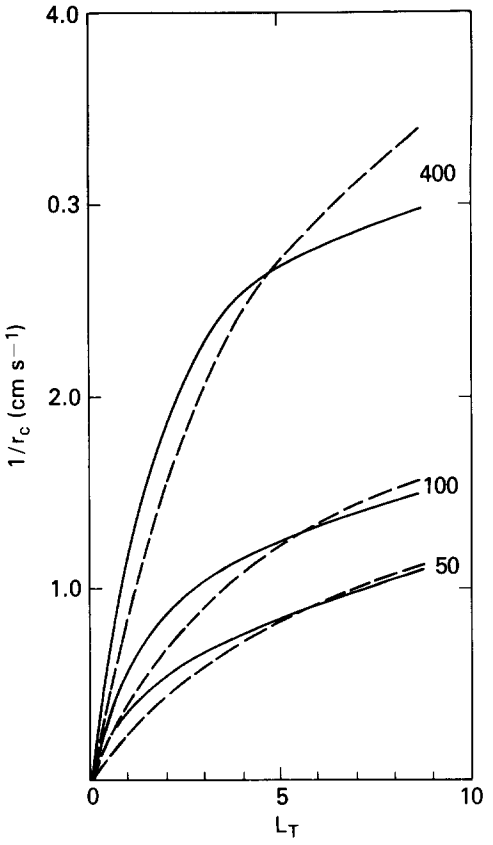

FIGURE 5. Inverse canopy resistance, $1/r_c$, as a function of leaf area index L_T, PAR flux density (marked against each curve in W m^{-2}), and leaf angle distribution (solid lines for horizontal leaves; dashed lines for spherical leaf angle distributions).

ties listed in Table 1. A point of contention in the solution of (12) and (13) is the use of the semiempirical description of PAR attenuation, (11), in place of the more exact two-stream description of the downward flux of PAR which is given by

$$F_L = F_0 \cdot \left[e^{-KL}(1 + h_4/\sigma) + h_5 e^{-hL} + h_6 e^{hL} \right], \quad (15)$$

which is obtained by combining the direct flux at L with the diffuse flux at the same level as given by (4b). However, for small values of ω, (11) and (15) give very similar results.

Figure 6(a) shows the *maximum* divergence between the predicted values of F_L as given by (11) and (15) for the canopy with horizontal leaves—it can be seen that the difference between the results of the two calculations is almost negligable. Also shown in Fig. 6 are the calculated profiles of leaf photosynthetic rates, P, and inverse stomatal resistances, $1/r_s$, down through the canopy calculated with

the two-stream, (15), and the exponential extinction, (11), formulations. The total equivalent canopy quantities, P_c and $1/r_c$, may be obtained by integrating the P and $1/r_s$ curves with respect to leaf area index L_T. It may be seen by eye that the difference between the photosynthetic rates and resistances as calculated by the two methods is almost insignificant, so justifying the use of (11) in (9) and (10).

Theoretical Discussion

Using the expression for canopy reflectance given by (5) and those for canopy photosynthesis and resistance, (9) and (10), Sellers (1985) compared the simple ratio and normalized difference of the vegetation index, hereafter referred to as SR and NDVI, respectively, to the equivalent estimates of P_c and $1/r_c$. For the sake of simplicity, we redefine SR and

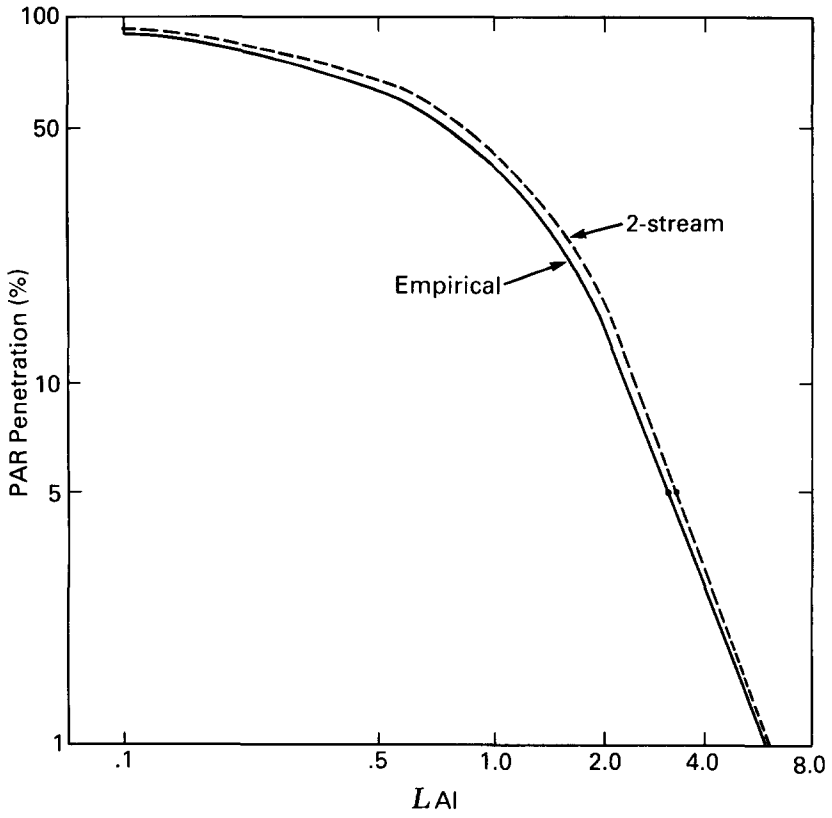

FIGURE 6. (a) PAR penetration against cumulative leaf area index LAI, as calculated by the two-stream model, Eq. (15), and the semiempirical extinction model of Goudriaan (1977), Eq. (11) (Horizontal leaves). (b) Leaf photosynthetic rates P against cumulative leaf area index LAI as calculated by the two-stream model, Eq. (15), and the semiempirical extinction model of Goudriaan (1977), Eq. (11), PAR flux descriptions. PAR flux above the canopy, F_0, 500 W m^{-2}. (Horizontal leaves). (c) Inverse leaf stomatal resistance $1/r_s$ against cumulative leaf area index LAI as calculated by the two-stream model, Eq. (15), and the semiempirical extinction model of Goudriaan (1977), Eq. (11), PAR flux descriptions. PAR flux above the canopy, $F_0 = 500$ W m^{-2}. (Horizontal leaves).

(b)

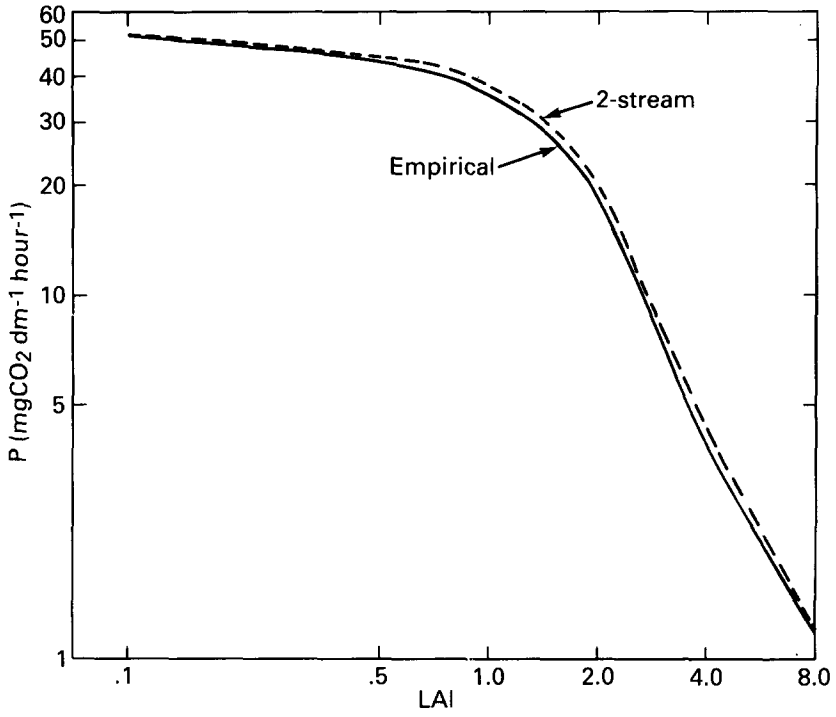

(c)

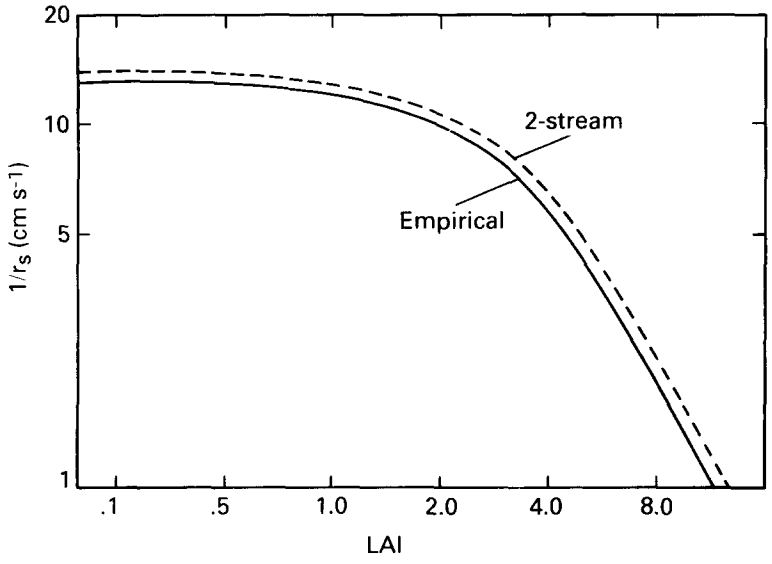

FIGURE 6. (Continued)

ND by

$$\mathrm{SR} = \frac{a_N}{a_V}, \tag{16a}$$

$$\mathrm{ND} = \frac{a_N - a_V}{a_N + a_V}, \tag{16b}$$

where

a_N, a_V = hemispherical canopy reflectances for the near-infrared and visible wavelength intervals, respectively [from (5)].

[*N.B.*: It should be noted that in the following discussion we define SR and ND in terms of surface reflectances rather than radiances, which are what remote sensing instruments measure. This simplifies the analysis considerably without any loss of physics. The relationship between reflectances and radiances is discussed in the last section of this paper.]

For the case of our model canopy with horizontal or "spherical" leaves, where $\omega_V = 0.2$ and $\omega_N = 0.8$ or 0.95 as described in Table 1, SR and ND both exhibit a nonlinear increase with leaf area index as shown in Fig. 2, with the rate of increase partly dependent upon the soil optical properties. It may be seen that the "signal" represented by the SR or ND becomes saturated, for all practical purposes, somewhere around a leaf area index of 5. Figure 2 may be compared to Figs. 3 and 5 where similar nonlinear responses for APAR, P_c, and $1/r_c$ vs. L_T may also be noted. Figures 7–9 compare the SR and ND with APAR, P_c, and $1/r_c$ directly, showing that for these cases at least (and we have every reason to believe it to be more or less generally true), the value of SR is near-linearly related to APAR, P_c, and $1/r_c$. [*Digression:* Figure 10 shows P_c and $1/r_c$ plotted against one another for a range of PAR flux densities. The near-linear relationship is to be expected from the work of Farquhar and von Caemmerer (1982), who proposed that stomatal resistance is optimally related to the leaf photosynthetic rate. Figure 10 merely shows that what is good for a leaf should naturally be good for a canopy and that the data in Table 1 are more or less consistent with the theoretical relationship.] Figures 7–9 and other similar results summarized from Sellers (1985) indicate strongly that

$$\mathrm{SR} \propto \mathrm{APAR}, \tag{17a}$$

$$\mathrm{SR} \propto P_c, \tag{17b}$$

$$\mathrm{SR} \propto 1/r_c. \tag{17c}$$

Obviously, (17) is a very useful result from a practical viewpoint. The phenomena encapsulated by Eq. (17) do not have immediately obvious explanations: Most of the rest of this paper is devoted to elucidating the biophysical processes that give rise to this relationship.

Given the fact of (17), we should look through our equation set for a common biophysical property linking the quantities SR, P_c, and $1/r_c$: Clearly, it can only be the total leaf area index L_T. It follows from this and (17) that

$$\frac{\partial(\mathrm{SR})}{\partial L_T} \propto \frac{\partial(\mathrm{APAR})}{\partial L_T}, \tag{18a}$$

$$\frac{\partial(\mathrm{SR})}{\partial L_T} \propto \frac{\partial P_c}{\partial L_T}, \tag{18b}$$

$$\frac{\partial(\mathrm{SR})}{\partial L_T} \propto \frac{\partial(1/r_c)}{\partial L_T}. \tag{18c}$$

The reason why (18) should hold is now to be discussed. To maintain some kind of organization in the discussion, we shall explore the dependence of the above derivatives in two following subsections; the first dealing with the left-hand side of

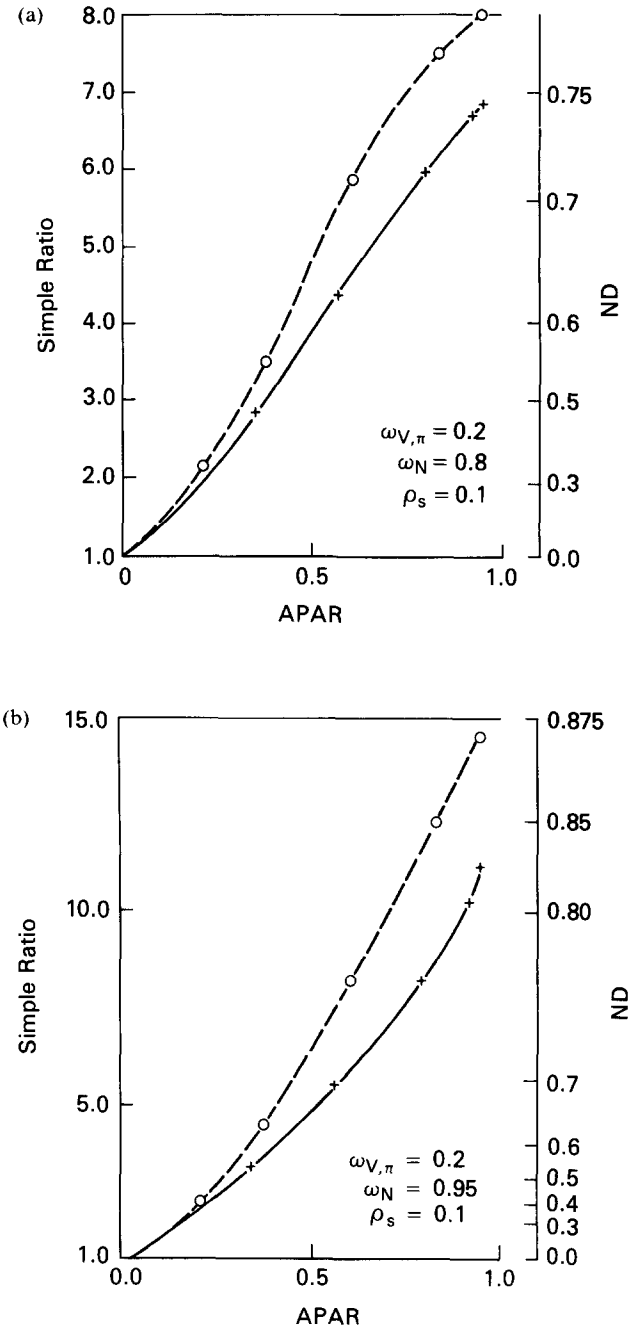

FIGURE 7. Simple ratio and the ND plotted against the absorbed fraction of photosynthetically active radiation (APAR). Background soil reflectance is 0.1. Solid lines denote horizontal leaves; dashed lines denote a spherical leaf angle distribution. Circles (○) and crosses (+) refer to increasing values of the total leaf area index L_T: O (origin), 0.5, 1.0, 2.0, 4.0, 8.0. (a) Simple ratio calculated using $\omega_N = 0.8$. (b) Simple ratio calculated using $\omega_N = 0.95$.

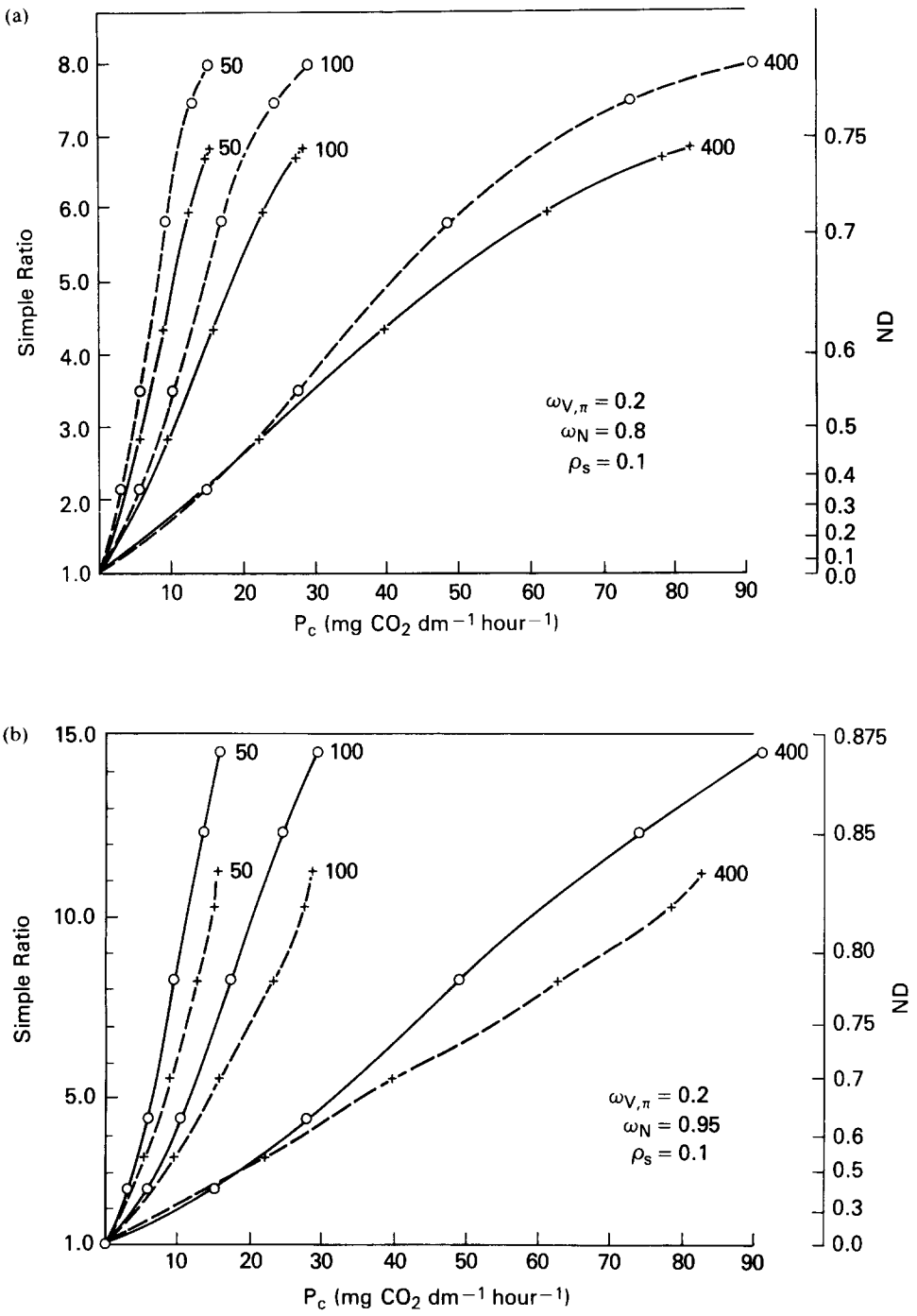

FIGURE 8. Simple ratio plotted against canopy photosynthetic rate P_c for different values of the PAR flux density, marked against each curve in W m^{-2}. Background soil reflectance is 0.1. Solid lines denote horizontal leaves; dashed lines denote a spherical leaf angle distribution. Circles (●) and crosses (+) refer to increasing values of the total leaf area index L_T: O (origin), 0.5, 1.0, 2.0, 4.0, 8.0. (a) Simple ratio calculated using $\omega_N = 0.8$. (b) Simple ratio calculated using $\omega_V = 0.95$.

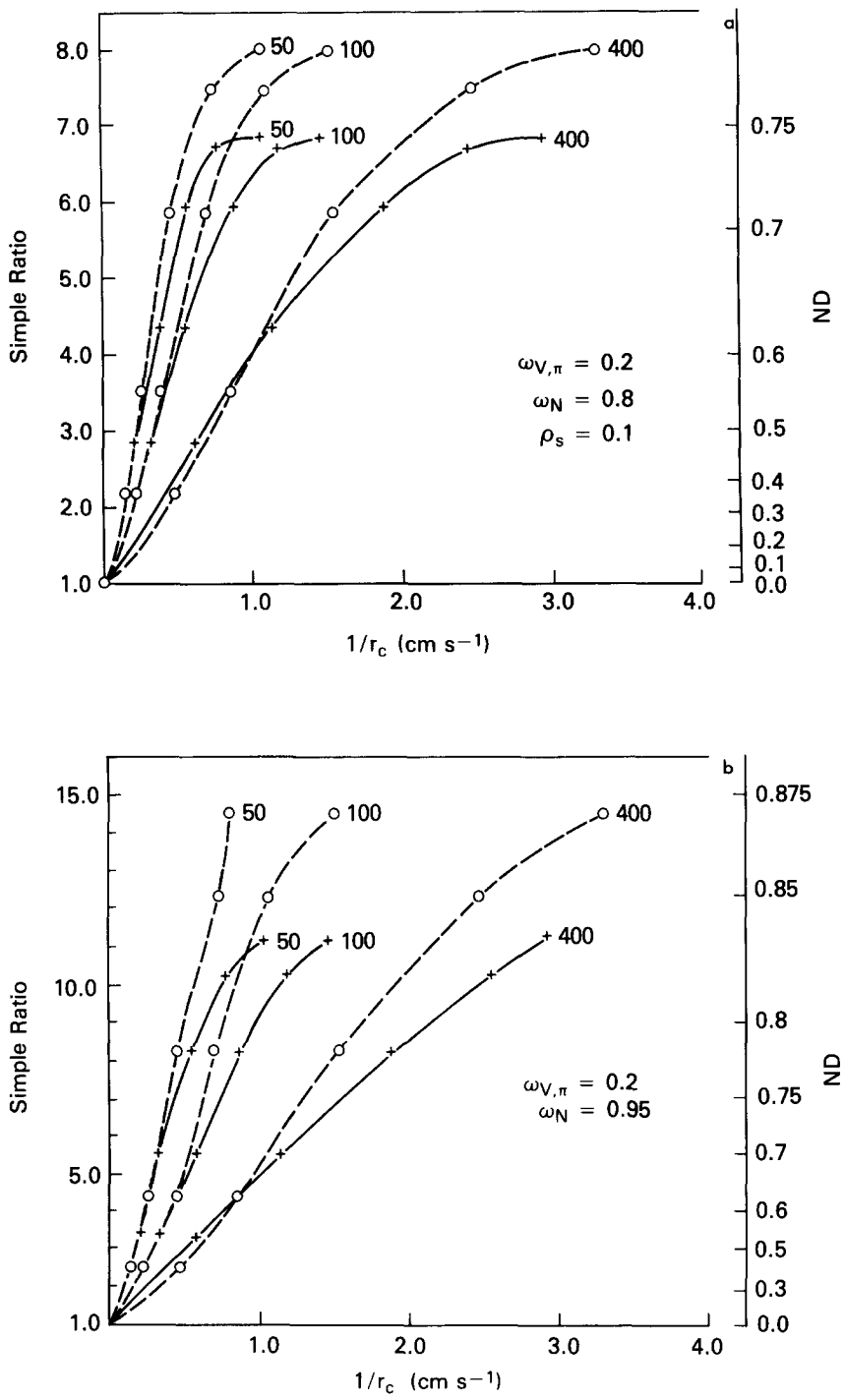

FIGURE 9. Simple ratio plotted against inverse canopy resistance $1/r_c$ for different values of the PAR flux density, marked against each curve in W m^{-2}. Other symbols and conditions are the same as for Fig. 8. (a) Simple ratio calculated using $\omega_N = 0.8$. (b) Simple ratio calculated using $\omega_N = 0.95$.

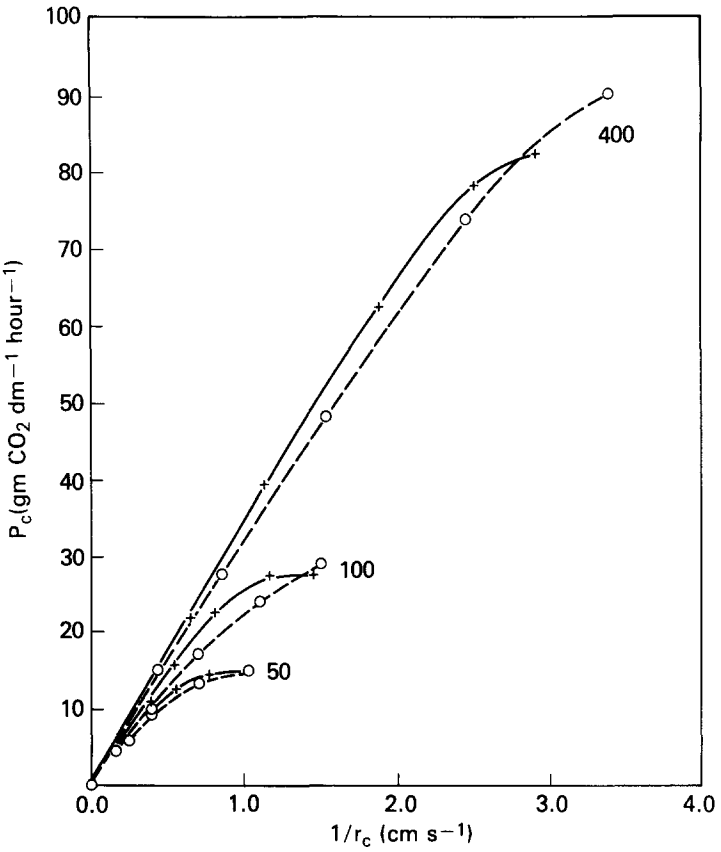

FIGURE 10. Canopy photosynthetic rate P_c, plotted against inverse stomatal resistance a/r_c, for different values of PAR flux density, marked against each curve in W m^{-2}. Solid lines denote horizontal leaves; dashed lines denote a spherical leaf angle distribution. Circles (●) and crosses (+) refer to total leaf angle indexes increasing from left to right: O (origin) 0.5, 1.0, 2.0, 4.0, 8.0.

(18), $\partial(\mathrm{SR})/\partial L_T$, the second with the right-hand side of (18), $\partial(\mathrm{APAR})/\partial L_T$, $\partial P_c/\partial L_T$, and $\partial(1/r_c)/\partial L_T$.

The dependence of the simple ratio (SR) upon total leaf area index (L_T)

Equation (16a) for SR may be differentiated with respect to L_T to give

$$\frac{\partial(\mathrm{SR})}{\partial L_T} = \frac{1}{a_V^2}\left(a_V\frac{\partial a_N}{\partial L_T} - a_N\frac{\partial a_V}{\partial L_T}\right). \quad (19)$$

It will be remembered that we are currently limiting the discussion to the consideration of canopies with horizontal and spherical leaf angle distributions. For the sake of brevity, we shall illustrate the expansion of the general case, (19), with reference to the horizontal leaf angle distribution in this text. An equivalent expansion for the spherical leaf angle distribution is given in the Appendix.

Canopy reflectance is given by (5). For a canopy of horizontal leaves, this reduces

to

$$a = \frac{\omega}{2}\left(\frac{1-A}{P_1 - P_2 A}\right), \qquad (20)$$

where

$$A = \left(\frac{P_1 - \gamma}{P_2 - \gamma}\right) e^{-2hL_T},$$

a = canopy reflectance,

ω = leaf scattering coefficient,

$P_1 = 1 - \omega/2 + h$,

$P_2 = 1 - \omega/2 - h$,

$h = (1-\omega)^{1/2}$,

$\gamma = \omega/2\rho_s$.

Intermediate steps between (5) and (20) are set out in the Appendix. It is clear from (20) that the canopy reflectance depends upon the leaf scattering coefficient divided by 2, adjusted by a term that includes a dependence on the soil scattering properties and the negative exponent of *twice* the total diffuse optical path length for a given value of L_T. This term, e^{-2hL_T}, is of fundamental importance to the rest of the discussion.

The derivative of (20) with respect to L_T, which is required in (19), is

$$\frac{\partial a}{\partial L_T} = \omega h A\left[\frac{P_1 - P_2}{(P_1 - P_2 A)^2}\right], \qquad (21)$$

intermediate steps again being given in the Appendix.

Some experimentation with typical values of leaf and soil scattering properties reveals that the near-infrared terms in (19) are the dominant ones in controlling the variation of SR with L_T. To emphasize the point, we may ask under what conditions may either $\partial a_N/\partial L_T$ or $\partial a_V/\partial L_T$ be identically zero. This will occur when $\gamma = P_1$ [see the definition of A in (20)] or, put another way, when

$$\frac{\omega}{2\rho_s} = 1 - \frac{\omega}{2} + h,$$

or

$$\rho_s' = \left[\frac{\omega}{2 - \omega + 2(1-\omega)^{1/2}}\right], \qquad (22)$$

where

ρ_s' = value of soil reflectance that makes $\partial a/\partial L_T = 0$.

The value of ρ_s' given by (22) is equal to the reflectance of an infinitely thick canopy; see Eq. (8) of Sellers (1985). When $\rho_s = \rho_s'$, the surface reflectance will show no change whether the soil is bare or is covered by the densest of canopies. This condition can be seen most clearly by inspecting Fig. 1.

It is interesting to note that for the visible wavelength interval, $\omega_V = 0.2$ and $\rho_s' = 0.0557$ for horizontal leaves while corresponding values for the near-infrared wavelength interval yield $\omega_N = 0.8$ and $\rho_s' = 0.38$ or $\omega_N = 0.95$ and $\rho_s' = 0.63$. Most soil reflectances lie within the range of 0.05–0.15 in the visible and 0.1–0.2 in the near-infrared. We can see then that normally $\partial a_V/\partial L_T$ is small, a_V itself is small and $\partial \mathrm{SR}/\partial L_T$ will depend primarily on $\partial a_N/\partial L_T$.

[*N.B.*: Soil reflectance in the near-infrared region seldom approaches the calculated ρ_s' value so the converse case of $\partial a_N/\partial L_T = 0$ should be rare. Areas where such light colored soils may be found are generally confined to deserts

or marginal zones where vegetation is sparse.]

From the above, we see that the first term in (19) tends to dominate the SR response to increases in L_T. The "interference" produced by the second term being nonzero will increase as the soil reflectance increases.

It has been stated that usually $\rho_s \simeq \rho_s'$ in the visible region so that (19) degenerates towards the approximation.

$$\frac{\partial(\mathrm{SR})}{\partial L_T} \to \frac{1}{a_V} \cdot \frac{\partial a_N}{\partial L_T} = \left(\frac{2P_1}{\omega}\right)_V \cdot \frac{\partial a_N}{\partial L_T}, \quad (\rho_s \to \rho_s')_V. \tag{23}$$

Clearly, the important functional term in (23) is the $e^{-2h_N L_T}$ embedded in $\partial a_N/\partial L_T$. An inspection of the preceding equation set will show that the $e^{-2h_N L_T}$ term, multiplied by a constant (as $\rho_{s_N} \to 0$, $A \to e^{-2h_N L_T}$) to form A, occurs *by itself* in the *numerator* of (21) and hence becomes the dominant functional term in (19) and (23). [The role of A in the *denominators* of (19) and (23) through its position in the denominator of (21) is subordinate as for the near-infrared case $P_2 < P_1$.]

From the above discussion, we see that:

i. The simple ratio and, by extension, the normalized difference vegetation indexes are primarily functions of the near-infrared reflectance under normal field conditions; that is, when $(\rho_s \to \rho_s')_V$.

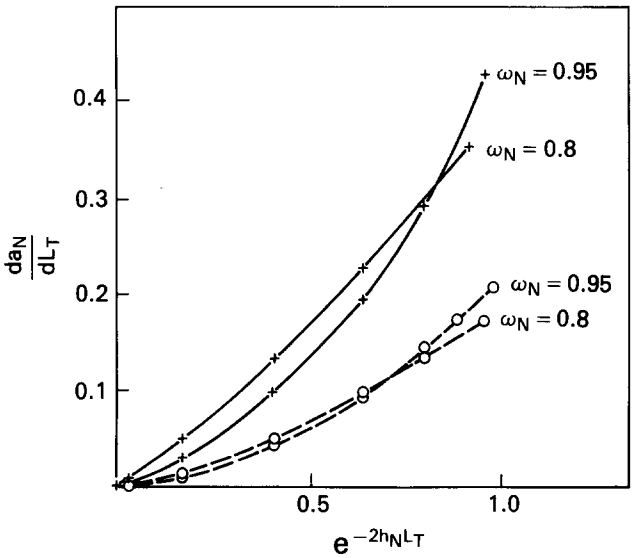

FIGURE 11. Variation of the derivatives of the near-infrared reflectance a_N, with respect to total leaf area index L_T with the square of the near-infrared penetration function, $e^{-2h_N L_T}$; $h_N = (1 - \omega_N)^{1/2}$. Solid lines denote horizontal leaves; dashed lines denote a spherical leaf angle distribution. Circle and crosses refer to values of L_T increasing from *right to left*: 0.1, 0.5, 1.0, 2.0, 4.0, 8.0. a_N is calculated for the two values of ω_N used in the study, 0.8 and 0.95. Soil reflectance is 0.1.

ii. The derivative of the simple ratio with respect to L_T is roughly proportional to $e^{-2h_N L_T}$ when $\rho_{s_N} \to 0$ (see Fig. 11). The mathematics for this result may be found in this paper and its appendix; the physical reason for it being so is that the reflectance is a function of twice the diffuse optical path length of the scattering medium—once for the attenuation of the radiation going into the medium (interception) plus once for its attenuation going out of the medium (backscatter or reflectance). In the visible region, this scattering effect has little effect on the reflected signal as dark soil and a vegetation canopy have similar reflectances. In the near-infrared region, the reflectance increases as $e^{-2h_N L_T}$ as the canopy and soil reflectance are normally dissimilar.

We may summarize these results by

$$\frac{\partial(\mathrm{SR})}{\partial L_T} \propto \frac{\partial a_N}{\partial L_T} \propto e^{-2h_N L_T}, \quad (\rho_s \to \rho_s')_V, (\rho_s \to 0)_N \quad (24)$$

where

h_N = total diffuse extinction coefficient for near infrared radiation,

$= (1 - \omega_N)^{1/2}$, assuming $\bar{\mu} = 1$

$= 0.4472$, when $\omega_N = 0.8$

$= 0.525$, when $\omega_N = 0.95$.

The dependence of the absorbed fraction of PAR (APAR), canopy photosynthesis (P_c) and resistance (r_c) on total leaf area index (L_T)

The derivative of APAR with respect to total leaf area index is obtained from (8) to give

$$\frac{\partial(\mathrm{APAR})}{\partial L_T} = -\frac{\partial a_\pi}{\partial L_T} - (1 - \rho_{s\pi})\frac{\partial}{\partial L_T} \times \left[e^{-K_\pi L_T} + I\downarrow(L_T)\right]. \quad (25)$$

For a canopy with horizontal leaves and a dark underlying soil, (25) simplifies to

$$\frac{\partial(\mathrm{APAR})}{\partial L_T} \simeq (1 - \rho_{s_\pi}) h_\pi e^{-h_\pi L_T} \propto e^{-h_\pi L_T}, \quad (\rho_s \to \rho_s' \to 0)_\pi. \quad (26)$$

If we use the semiempirical expression for PAR flux attenuation, (11), in place of the two-stream description, (26) becomes

$$\frac{\partial(\mathrm{APAR})}{\partial L_T} \propto e^{-kL_T}, \quad (\rho_s \to \rho_s' \to 0)_{V,\pi}. \quad (27)$$

Figure 12 shows the APAR derivative, calculated from the complete expression of (25), plotted against e^{-kL_T} for the two leaf angle distributions and two values of the soil reflectance. The relationship of (26) and (27) is clearly best satisfied when $(\rho_s \to \rho_s' \to 0)_{V,\pi}$. However, even fairly high values of ρ_{s_V} do not degrade the relationship too seriously.

For the simple case of horizontal leaves, the derivatives of P_c and $1/r_c$ with respect to L_T are simply

$$\frac{\partial P_c}{\partial L_T} = \frac{a_1 F_0 e^{-kL_T}}{b_1 + F_0 e^{-kL_T}}, \quad (28)$$

$$\frac{\partial(1/r_c)}{\partial L_T} = \frac{b_2 + F_0 e^{-kL_T}}{a_2 + c_2(b_2 + F_0 e^{-kL_T})}. \quad (29)$$

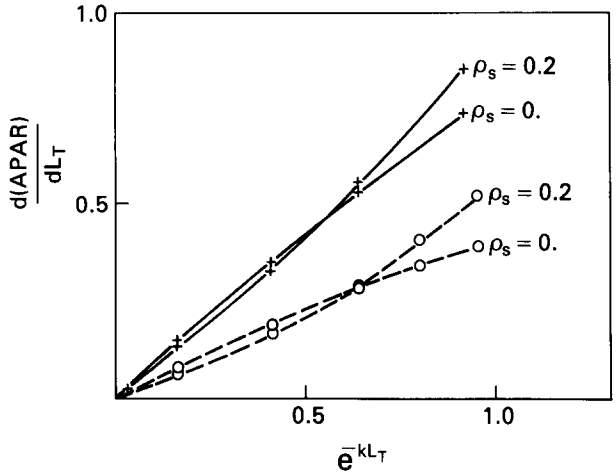

FIGURE 12. Derivative of APAR with respect to total leaf area index L_T plotted against the PAR penetration function e^{-kL_T}, k = PAR attenuation coefficient, $= G(\mu)/\mu(1-\omega_\pi)^{1/2}$. The relationships are shown to be near-linear for low soil reflectances ($\rho_s = 0$) and become increasingly nonlinear for increasing soil reflectance ($\rho_s = 0.2$). Solid lines denote horizontal leaves; dashed lines denote a spherical leaf angle distribution. Circles and crosses refer to values of L_T, increasing from *right to left*: 0.1, 0.5, 1.0, 2.0, 4.0, 8.0.

The derivation of (28) and (29) may be found in Sellers (1985): A quick check of their correctness may be made by taking the finite difference forms of the left-hand sides; so, for example, $\partial P_c/\partial L_T$ becomes $\Delta P_c/\Delta L_T$, and transferring the ΔL_T term to the right hand side. The resulting expressions may then be compared with (9) and (10). Equivalent expressions to (28) and (29) for other leaf angle distributions may be obtained from Sellers (1985). Generally speaking, all of them show a strong dependence on the e^{-kL_T}.

Figures 13 and 14 show the variation of the derivative terms in (28) and (29) with e^{-kL_T}. Clearly, the relationship is almost linear as PAR $\rightarrow$ 0, which reduces the exponential terms in the denominators of (28) and (29) to insignificance. As the PAR flux density increases, ($F_0 = 400$ W m^{-2} represents the maximum one could expect to observe in nature) the relationship becomes increasingly nonlinear as the plants photosynthetic capacity approaches saturation. In practice, however, most indigenous species in a region reach PAR saturation at around the maximum local PAR flux density (see Farquhar and von Caemmerer, 1982).

The relationships represented by Eqs. (27)–(29) and Figs. 12–14 are entirely self-consistent. At the risk of laboring the obvious, we should expect APAR, P_c, and $1/r_c$ to be closely linked as the plants' demand for CO_2 and the associated rate of water vapor loss are functional on the supply side of the electron transfer process of photosynthesis, which is directly related to chlorophyll density and hence APAR.

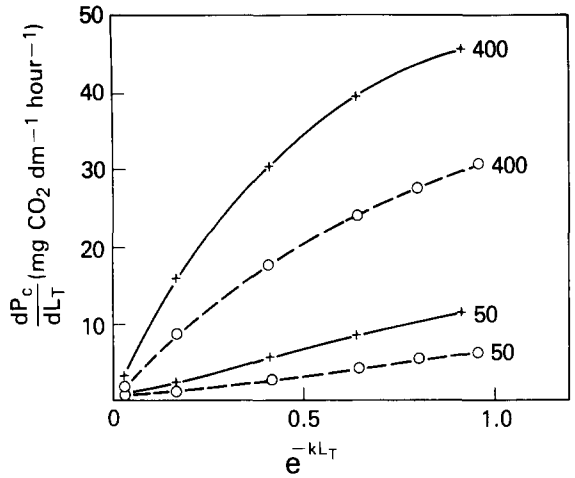

FIGURE 13. Derivative of canopy photosynthetic rate P_c with respect to total leaf area index L_T against PAR penetration function e^{-kL_T}. PAR flux densities are marked against each curve in W m^{-2}. Symbols and conditions are the same as for Fig. 12.

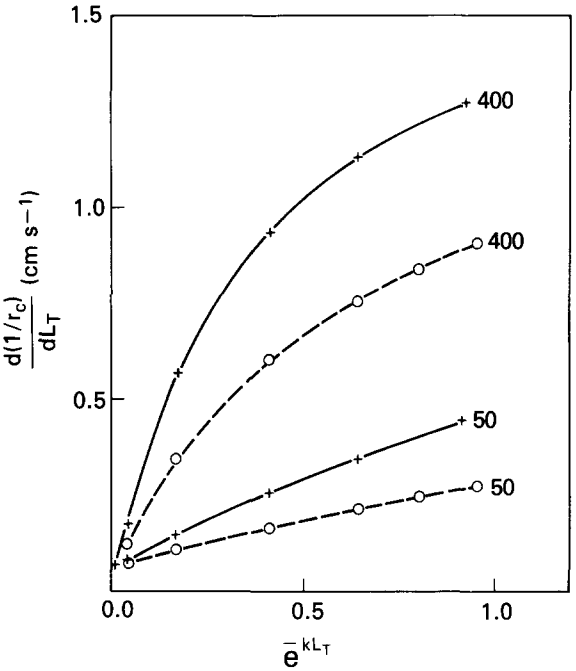

FIGURE 14. Derivative of inverse stomatal resistance $1/r_c$ with respect to total leaf area index L_T against PAR penetration function, e^{-kL_T}. PAR flux densities are marked against each curve in W m^{-2}. Symbols and conditions are the same as for Figs. 12 and 13.

We may summarize all the above by

$$\frac{\partial(\text{APAR})}{\partial L_T}, \frac{\partial P_c}{\partial L_T}, \frac{\partial(1/r_c)}{\partial L_T} \propto e^{-kL_T}, \quad (F_0 \to 0,\ \rho_s \to \rho_s' \to 0)_V, \qquad (30)$$

where

k = semiempirical extinction coefficient for PAR
$= G(\mu)/\mu(1-\omega_\pi)^{1/2}$
$= 0.8944$ for horizontal leaves
$= 0.4472$ for spherically distributed leaves.

The physical explanation for (30) is that PAR is utilized by the canopy as it is attenuated down through it. P_c and $1/r_c$ are therefore related to the *one way* passage of PAR down through the canopy as described by the e^{-kL_T} term.

The relationship between the simple ratio (SR), the absorbed fraction of PAR, (APAR), canopy photosynthesis (P_c), and canopy resistance (r_c)

Previously in this paper, it was pointed out that data and modelling had indicated a near-linear relationship, Eq. (17), between SR and APAR, P_c, and $1/r_c$ for the normal field situation. The necessary condition for this phenomenon was summarized by Eq. (18). Clearly (18) can only hold when the ratio of the right-hand sides of (24) and (30) is constant. As a reminder, (24) and (30) are

$$\frac{\partial(\text{SR})}{\partial L_T}, \frac{\partial a_N}{\partial L_T} \propto e^{-2h_N L_T}, \qquad (24)$$

$$\frac{\partial(\text{APAR})}{\partial L_T}, \frac{\partial P_c}{\partial L_T}, \frac{\partial(1/r_c)}{\partial L_T} \propto e^{-kL_T}. \qquad (30)$$

For their ratio to be constant for all values of L_T, we must have

$$e^{-2h_N L_T} = e^{-kL_T}, \qquad (31a)$$

which leads to

$$2h_N = k, \qquad (31b)$$

$$2(1-\omega_N)^{1/2} = \frac{G(\mu)}{\mu}(1-\omega_\pi)^{1/2}, \qquad (31c)$$

and

$$\omega_N = 1 - \left[\frac{G(\mu)}{2\mu}\right]^2 (1-\omega_\pi). \qquad (31d)$$

For the worked examples discussed in this paper, we have the following relationships:

Horizontal leaves:

$$\omega_\pi = 0.2,$$
$$G(\mu)/\mu = 1,$$

so that, to satisfy (31), $\omega_N = 0.8$,

Spherically distributed leaves:

$$\omega_\pi = 0.2,$$
$$G(\mu)/\mu = 0.5 \quad \text{(for an overhead sun)}$$

so that, to satisfy (31), $\omega_N = 0.95$.

The significance of the above is as follows: If we wish to infer APAR, P_c, or $1/r_c$ from surface reflectance measurements, we should choose spectral bands in the near-infrared that come close to satisfying (31). It so happens that for the common cases of spherical and horizontal leaf angle distributions, the values of ω_N produced by (31) are close to those observed in the 0.7–1.1 μm and 1.6–1.8 μm regions, respectively.

Figures 15–17 show the derivatives of APAR, P_c, and $1/r_c$ with respect to L_T plotted against the derivative of the near-infrared reflectance, a_N. A close inspection of Fig. 15 will show that when $\omega_N = 0.8$, the linearity between APAR and a_N is best for horizontal leaves and that when $\omega_N = 0.95$, the linearity is best for spherically distributed leaves. The same trend is apparent in Fig. 7, where SR is plotted against APAR. In Figs. 16 and 17, the derivatives of P_c and $1/r_c$ are plotted against the "optimal" values of $\partial a_N/\partial L_T$, where $\omega_N = 0.8$ for horizontal leaves and $\omega_N = 0.95$ for the spherical leaf angle distribution. An inspection of Figs. 8 and 9 will show, however, that (31) holds here as well; the relationships are more linear when (31) is exactly satisfied.

The result of (31) is the most important finding of this study. The preceding analysis and (31) state that if:

i. the spectral properties of green leaves were to conform to the condition specified by (31),
ii. the canopy consisted of randomly positioned leaves, and
iii. the soil was dark so that $(\rho_s \rightarrow \rho_s')_V$, $(\rho_s \rightarrow 0)_N$,

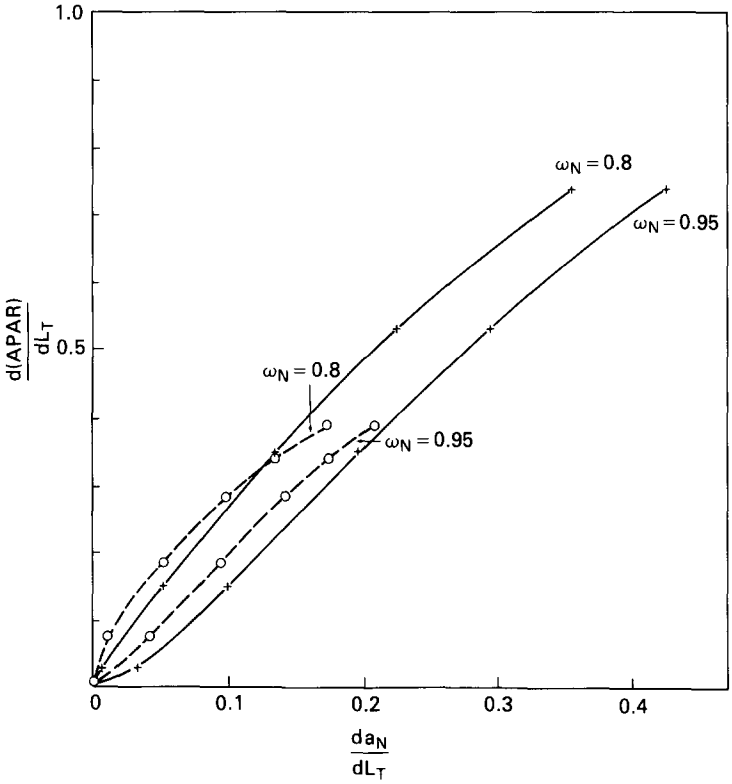

FIGURE 15. Derivatives of APAR and near-infrared reflectance a_N with respect to total leaf area index L_T plotted against each other. Solid lines denote horizontal leaves; dashed lines denote a spherical leaf angle distribution. Circles and crosses refer to values of L_T increasing from right to left: 0.1, 0.5, 1.0, 2.0, 4.0, 8.0. $\partial a_N/\partial L_T$ was calculated for the two values of ω_N 0.8 and 0.95, as marked on the figure. Soil reflectance is 0.1.

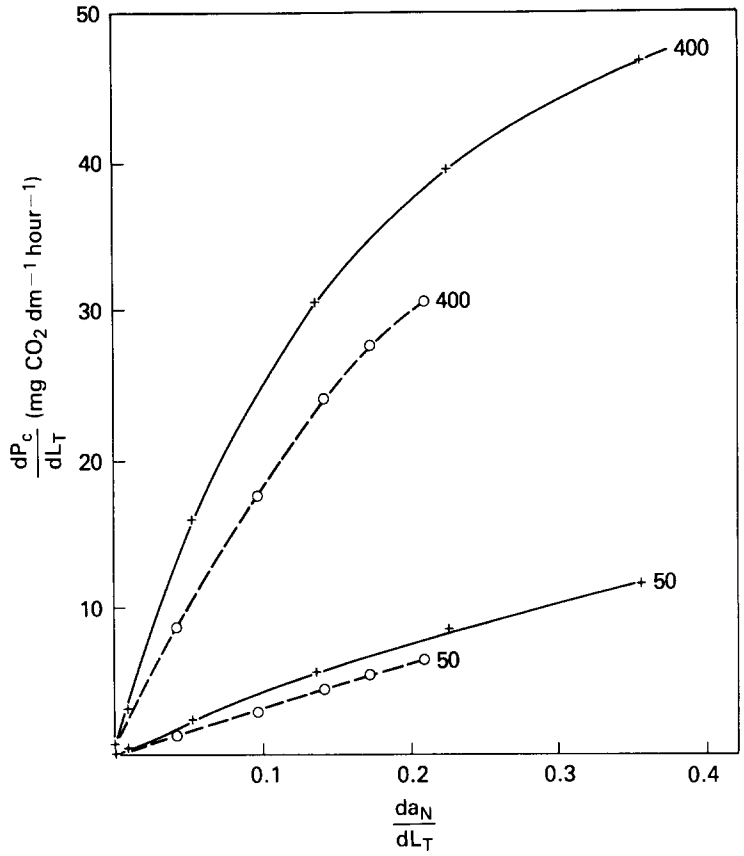

FIGURE 16. Derivatives of the canopy photosynthetic rate P_c and the near-infrared reflectance a_N, with respect to total leaf area index L_T, plotted against each other. All other symbols and conditions are the same as in Fig. 15.

spectral observations of the canopy reflectance would exhibit the following characteristics:

i. the near-infrared reflectance would be a near-linear indicator of APAR and a near-linear indicator of P_c and $1/r_c$ under stress-free conditions,

ii. the SR would be functional on the near-infrared reflectance only,

iii. surface reflectance in the visible region would be invariant with leaf area index.

All of the above may be expressed more prosaically. If an experimenter were somehow to launch an equal number of visible/PAR and near-infrared photons at a vegetated surface, he could estimate the number of visible/PAR photons absorbed by the vegetation (as opposed to the soil) by counting the reflected near-infrared photons rather than the reflected visible/PAR photons. The relationship between the two would be most linear under the ideal conditions we have specified above in (31).

The next section discusses the feasibility of applying reflectance data to the estimation of APAR, P_c, and $1/r_c$. In particular, the limitations imposed by the

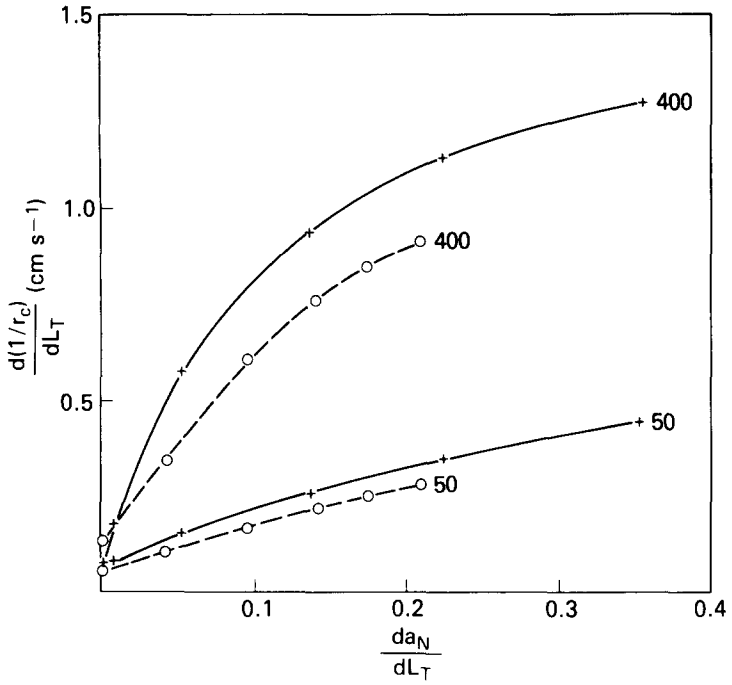

FIGURE 17. Derivatives of inverse stomatal resistance $1/r_c$ and the near-infrared reflectance a_N with respect to total leaf area index L_T, plotted against each other. All other symbols and conditions are the same as in Fig. 15.

architecture of real plant canopies and the configuration of operational satellite sensor systems are examined in the context of satisfying the condition of (31).

Applications

It has been shown that the near-linear relationship between canopy photosynthesis P_c, canopy inverse resistance $1/r_c$, and the simple ratio (SR) as observed in one form or another by Monteith (1977), Goward et al. (1985), and Sellers (1985) is due to the near conformism of the visible and near-infrared scattering coefficients for green foliage to the rule specified in (31). It is suggested that the biophysical explanation for the near-linear relationships between SR and P_c, $1/r_c$, and APAR is that the reflected near-infrared radiation is largely dependent on *twice* the optical path length for diffuse radiation in this wavelength interval, while P_c and $1/r_c$ are related to the *one way* attenuation of PAR on its passage down through the canopy, i.e., once times the direct beam path length for PAR flux. The linearity for the relationship arrives from the fortunate proportion of ω_V to ω_N for green leaves which more or less corresponds to the ideal relation expressed in (31).

It is important to ask at this point whether the real world is really comparable to the idealized case discussed up to now. Figure 18 shows the reflectance and transmittance spectra of green maize leaves together with a surface solar intensity spectrum S_λ for a typical midlatitude clear day taken from Miller (1972). Also

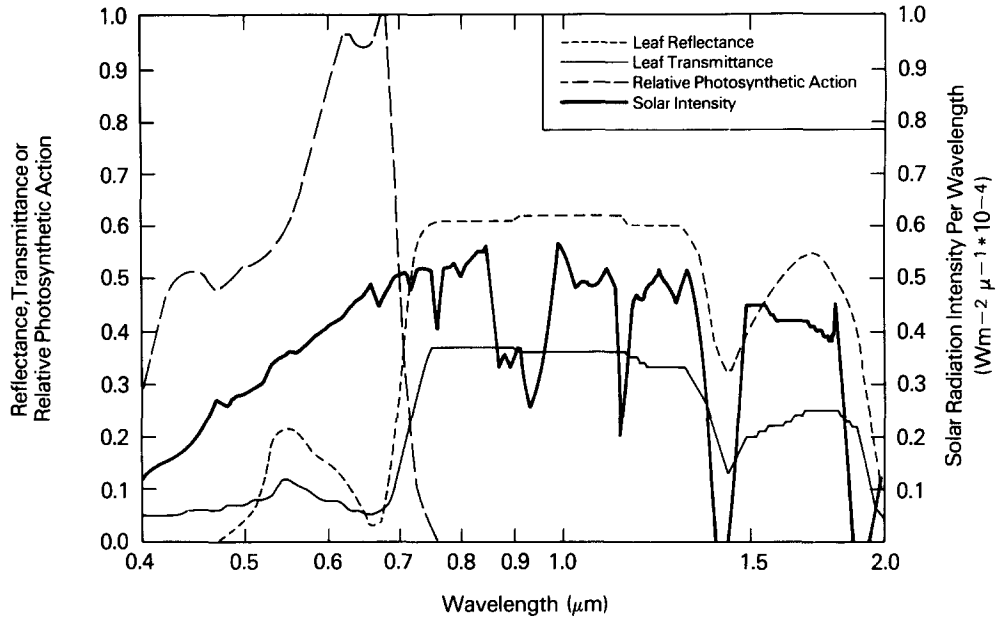

FIGURE 18. Maize leaf reflectance α and transmittance τ spectra for the range 0.4–2.0 μm. Also shown are the mean photosynthetic action efficiency spectrum for a number of species' leaves, C, and the incident solar flux at the surface of a clear day, S, in W m^{-2} μm^{-1}. α, τ, and S are from Miller et al. (1972); C is from McCree (1972).

shown is the mean action efficiency of photosynthesis (energy basis), C_λ, of a number of crop plants reported by McCree (1972). This action spectrum does not differ too widely from species to species as all green plants (C_3 and C_4) utilize the same initial photosynthetic fixation reaction. We may then calculate an "effective" PAR scattering coefficient for leaves, ω_π, by integrating the product of the action efficiency, C_λ, and the spectral scattering coefficient (reflectance plus transmission), over all wavelengths with a suitable weighting for the intensity of the incident solar radiation S_λ:

$$\omega_\pi = \frac{\int_0^\infty (\tau_\lambda + \alpha_\lambda) S_\lambda C_\lambda \, d\lambda}{\int_0^\infty S_\lambda C_\lambda \, d\lambda}, \quad (32)$$

where

$\tau_\lambda, \alpha_\lambda$ = leaf spectral transmittance, reflectance from Fig. 18,

$\tau_\lambda + \alpha_\lambda = \omega_\lambda$,

S_λ = incident solar flux intensity per wavelength $(\mathrm{W\,m^{-2}\,\mu m^{-1}})$,

C_λ = action efficiency of photosynthesis,

λ = wavelength (μm).

The equivalent broadband near-infrared scattering coefficient $\bar{\omega}_N$ is given by removing the C_λ terms and integrating (32) between limits of 0.68–2.0 μm. Using the data in Fig. 18, a numerical calculation of the quantities ω_π and $\bar{\omega}_N$

yielded values of 0.207 and 0.848, respectively: This combination is not too far from the ideal of (31) for a planophile canopy; see the square marked $\omega_{PAR}, \omega_{NIR}$ in Fig. 20. However, remotely sensed observations are seldom made across such broad bands. Figure 19 shows the relative spectral responses R_λ of the advanced very high resolution radiometer (AVHRR) mounted on the National Oceanic and Atmospheric Administration (NOAA) series of polar orbiting satellites and the R_λ curves for the multispectral scanner (MSS) and thematic mapper (TM) sensors mounted on the Landsat series of satellites. These data were obtained from Kidwell (1981), Markham and Barker (1983), and Markham and Barker (1985), respectively. The mean leaf scattering coefficients as observed using any one of these sensors may be calculated by

$$\bar{\omega} = \frac{\int_0^\infty (\tau_\lambda + \rho_\lambda) S_\lambda R_\lambda \, d\lambda}{\int_0^\infty S_\lambda R_\lambda \, d\lambda}, \quad (33)$$

where

R_λ = relative spectral response of satellite sensor as a function of wavelength.

Table 2 lists the values of $\bar{\omega}$ as calculated for each sensor using (33) and numerically integrating the functions over 0.01 μm intervals.

Of principal interest now is the question of which combination of two sensors is likely to give the best estimate of P_c and $1/r_c$, assuming that these are the

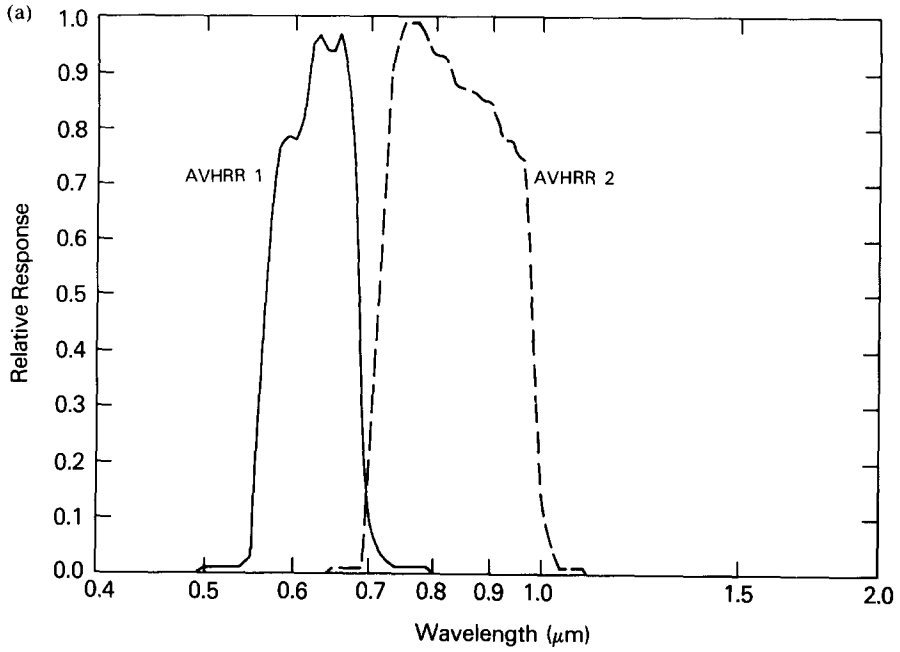

FIGURE 19. Relative spectral responses of: (a) Advanced Very High Resolution Radiometer (AVHRR), bands 1 and 2; (b) Multispectral Scanner (MSS), bands 1, 2, 3 and 4; (c) Thematic Mapper (TM), bands 1, 2, 3, 4, and 5.

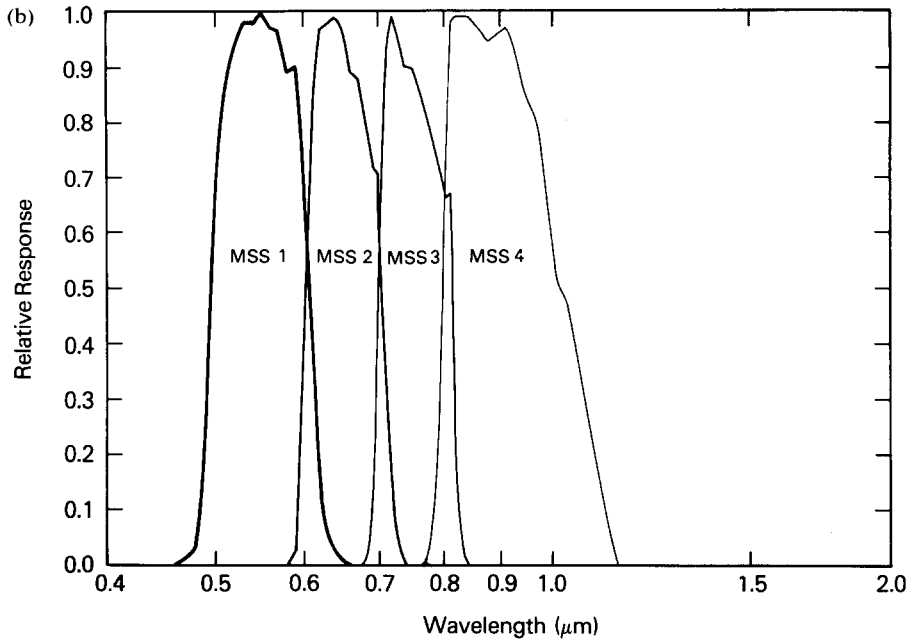

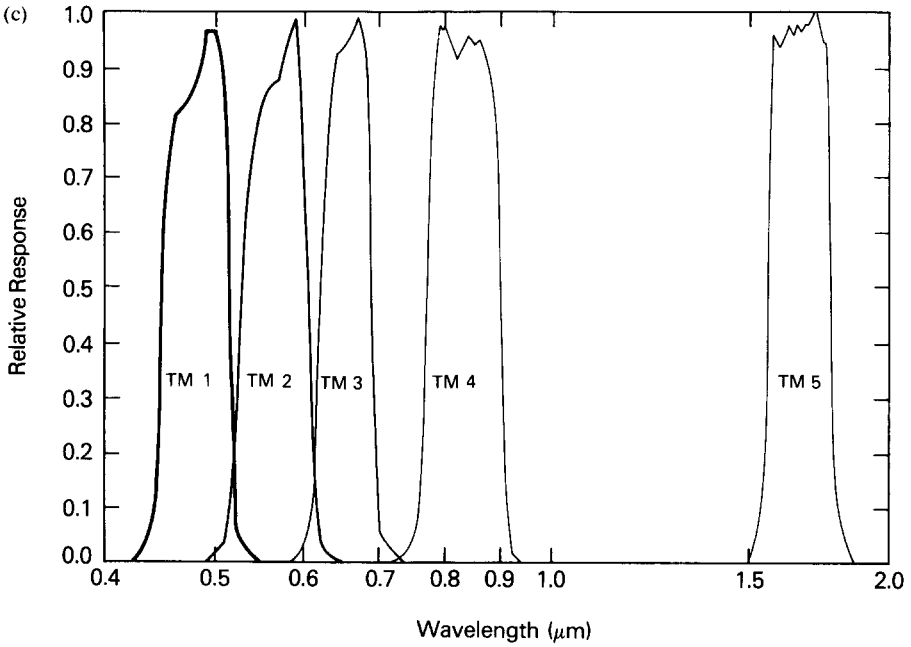

FIGURE 19. (Continued)

vegetation quantities of most concern to terrestrial ecologists, agronomists, climatologists, etc. The criteria which we should use to choose appropriate response functions for our two sensors are simply:

i. *Visible or PAR region sensor* $[R_\lambda]_V$. The apparent visible mean leaf scattering coefficient $\bar{\omega}_V$ as given by the sensor properties $[R_\lambda]_V$ and the spectral solar flux S_λ in (33) should come close to satisfying (22). This means that the resulting semi-infinite canopy reflectance observed in this spectral region would match the soil reflectance $(a \to \rho_s')_V$ so that the total surface reflectance would be invariant with vegetation density. In practical terms, it is impossible to select a single sensor for this task as the background soil reflectance varies widely over the globe. Probably the next best thing is to choose a value of $\bar{\omega}_V$ that approaches ω_π, which would ensure a good contrast between $\bar{\omega}_V$ and $\bar{\omega}_N$. This can be achieved by having the sensor response function $(R_\lambda)_V$ match the photosynthetic action efficiency function C_λ, thus making the sensor electronically equivalent to a green leaf.

ii. *NIR region sensor* $[R_\lambda]_N$. The apparent near-infrared mean leaf scattering coefficient $\bar{\omega}_N$ as given by the sensor properties $[R_\lambda]_N$ should fall as close to the value defined by (31), i.e., $\{1 - [G(\mu)/2\mu]^2(1 - \omega_\pi)\}$, as possible.

It should be noted that the criteria posited by i and ii above relate *only* to the objective of obtaining estimates of the area-averaged canopy photosynthetic capacity and inverse resistance via a simple transform applied to surface reflectance data. It is likely that these two criteria will predict "optimal" band mixes which are some way from being ideal with regard to other factors: for example, atmospheric effects, spectral contrast between sparse vegetation and bare soil, etc.

Figure 20 shows the above two criteria as lines in the $\bar{\omega}_V, \bar{\omega}_N$ domain. The optimum point, i.e., the best combination of $\bar{\omega}_V$ and $\bar{\omega}_N$, may be found at their intersections. Various combinations of each satellite sensor configuration are plotted in the same domain and their proximity to the optimum points may be taken as a rough indication as to the linearity of the resultant SR vs. APAR, P_c, and $1/r_c$ relationship.

Figure 20 clearly illustrates that the choice of an "optimal" near-infrared sensor is dependent upon the leaf angle distribution as well as ω_π. It is desirable that the visible, or PAR region, sensor is close to the ω_π line, marked on Fig. 20 as (i), a criterion satisfied by the AVHRR-1, MSS-1, and MSS-2 bands very well and by the TM-1, TM-2 and TM-3 bands moderately well. (Combinations of these TM bands would achieve the desired result.) Of the near and middle-infrared bands, TM-5 and MSS-3 satisfy (31) for horizontal leaves, line (iia), AVHRR-2 for spherically distributed leaves, line (iic). Since, in reality, we are constrained to the use of sensor combinations mounted on the same satellite (the problems associated with matching different viewing times and atmospheric conditions associated with data from two or more satellites are fairly severe), we should look for the single-satellite sensor combination that best satisfies the criteria mentioned above for the most common canopy geometries

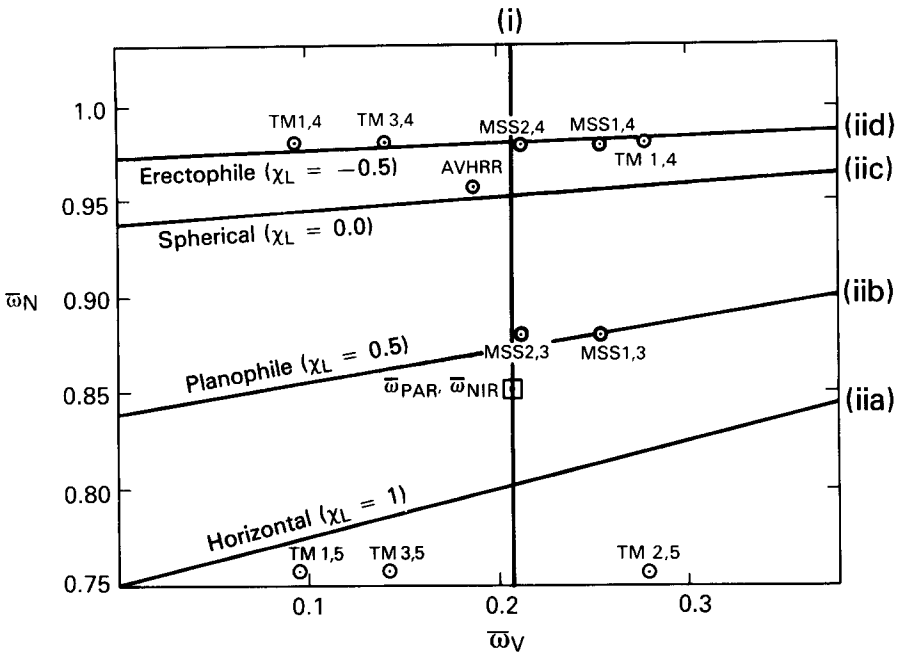

FIGURE 20. Plot of apparent visible $\bar{\omega}_V$, and near-infrared $\bar{\omega}_N$ scattering coefficients of green maize leaves as would be measured by different mixes of AVHRR, MSS, and TM bands using Eq. (33). The letters next to each point on the figure refer to an instrument (e.g., TM = Thematic Mapper) and the two numbers separated by commas refer to individual sensors on the instrument; the first number relating to the sensor operating in the visible region. If orthogonal lines are drawn linking each point to the figure axes, the ω values for each sensor as calculated by Eq. (33) may be read off. For example, the point labelled TM 1,4 refers to the Thematic Mapper where the visible region sensor (TM-1) is projected to give a value of 0.094 for $\bar{\omega}_V$ and the NIR region sensor (TM-4) is projected to give a value of 0.980 for $\bar{\omega}_N$ (see Table 2).

Also shown, as a straight vertical line labelled (i), is the value of ω_π as calculated from (32) in the text. Proximity of the sensor points to this vertical line indicates that the visible region sensor has a response function similar to the photosynthetic action efficiency curve shown in Fig. 18. The lines running from left to right on the figure, (iia)–(iid), represent solutions to (31) for four different leaf angle distributions: (iia) horizontal leaves (χ_L=1), (iib) planophile leaves (χ_L=0.5; see Appendix), (iic) spherically distributed leaves (χ_L = 0), and (iid) erectophile leaves (χ_L = − 0.5). Broadly speaking, the leaf angle distribution tends from horizontal to near-vertical from (iia) to (iid). Each line in (ii) represents the optimal relationship between $\bar{\omega}_N$ and $\bar{\omega}_V$ for the stated leaf angle distribution. Proximity of a sensor combination point to one of these indicates the suitability of the near-infrared sensor for biophysical analyses as defined by Eq. (31) in the text. Clearly, an optimal sensor combination would be close to line (i) and line (iic), representative of a spherical leaf angle distribution. It can be seen that the AVHRR combination falls very close to this optimal point.

found in nature, i.e., spherical or near-spherical leaf angle distributions. Two very strong candidates immediately emerge:

The first is the combination of the AVHRR channels which comprise the best possible two-sensor mix for spherically distributed leaves. The second is made up of MSS-2, in the visible region, and a mix of MSS-3 and MSS-4 in the near-infrared region which can be combined in various ways to give an optimal system for a range of leaf angle distributions. Combinations of TM-1, TM-2, and

TABLE 2 (a) Effective PAR Scattering Coefficient $\bar{\omega}_\pi$ and Broad Band Near-Infrared Scattering Coefficient ω_{NIR}, for Maize Leaves (from Fig. 18) and Eq. (33) in Text. (b) Apparent Visible $\bar{\omega}_V$, and near-infrared $\bar{\omega}_N$, Scattering Coefficients for Maize Leaves, as Would Be Measured by Satellite Sensors[a]

(a)	$\bar{\omega}_\pi$	$\bar{\omega}_{NIR}$
Maize leaves	0.207	0.848
(b)	$\bar{\omega}_V$	$\bar{\omega}_N$
AVHRR 1	0.187	—
AVHRR 2	—	0.956
MSS 1	0.254	—
MSS 2	0.212	—
MSS 3	—	0.880
MSS 4	—	0.980
TM 1	0.094	—
TM 2	0.278	—
TM 3	0.141	—
TM 4	—	0.980
TM 5	—	0.756

[b] Relative spectral response data of sensors taken from Fig. 15; originally from Kidwell (1978) for AVHRR, Markham and Barker (1983) for MSS and Markham and Barker (1985) for TM.

TM-3 can be used to synthesize a band that falls on the ω_π line, i.e., criterion (i). The TM-4 and TM-5 bands according to (31) are placed at the two extremes of possible canopy geometries: planophile and erectophile. In view of this, it is possible that a mix of TM-4 and TM-5 bands may be used to infer something about canopy geometry.

The obvious suitability of the AVHRR sensor combination is a surprising and encouraging result. Surprising, because the sensor was not designed with any biophysical tasks in mind and encouraging in that it strongly supports the global biophysical analyses performed by Fung et al. (1986) and Goward et al. (1986), and the interpretative work of Tucker et al. (1981). If, on the basis of Eq. (31), we were to design a satellite sensor system to carry out inventories of global scale photosynthetic capacity and minimum stomatal resistance, we would probably end up with something very close to the AVHRR instrument.

Summary and Conclusions

The near-linear dependence of canopy photosynthesis P_c on contemporaneous simple ratio (SR) or normalized difference (ND) data has been remarked on and used by a number of researchers working with remote sensing data, e.g., Goward et al. (1985). Using simple models of canopy radiative transfer, photosynthesis, and stomatal resistance we have seen that the spectral properties of plant leaves conform approximately to the rule:

$$2(1-\omega_N)^{1/2} = [G(\mu)/\mu](1-\omega_\pi)^{1/2}, \tag{31c}$$

which, if exactly satisfied, would ensure a near-linear relationship between canopy near-infrared reflectance a_N and APAR, P_c, and $1/r_c$ when the soil is relatively dark. In the visible region, soil reflectance is typically of the same magnitude as the asymptotic canopy reflectance, so that the SR and ND are mainly functional on a_N and the same linear relationship more or less holds good for them too. Physically, the reason for this serendipity is that while P_c and $1/r_c$ are roughly dependent on the one-way passage of PAR down through the canopy; a_N, SR, and ND are dependent on the two-way (inwards and out again) passage of near-infrared radiation. This accounts for the factor of 2 in (31) while the discontinuity in ω at 0.68 μm makes the square-rooted term on the right-hand side of (31) roughly twice that on the left. Of the satellite

instruments in operation, the Multispectral Scanner and AVHRR sensors would probably provide the best, i.e., most linear, most reliable, indication of APAR, P_c, and $1/r_c$ in the absence of atmospheric effects.

In view of the preceding discussion, it should occur to the alert reader that since a_N is the best indicator of APAR, P_c, and $1/r_c$, why should we bother with simple ratios and normalized differences which involve the additional term a_V? One reason (which has undoubtedly been expounded before and which is presented here only for the sake of completeness) is that remote sensing systems only measure radiances, not reflectances. Since these radiances are the product of an incident flux and a directional reflectance, the remotely sensed measurement is really providing the observer with the product of at least two unknowns. However, under normal terrestrial illumination conditions, it can be assumed that the ratio of incident visible and near-infrared fluxes is more or less constant so that

$$\int_0^\infty S_\lambda [R_\lambda]_V d\lambda = B \int_0^\infty S_\lambda [R_\lambda]_N d\lambda \tag{34}$$

where

B = const,

$[R_\lambda]_V$ = relative spectral response function of satellite sensor operating in the visible wavelength region,

$[R_\lambda]_N$ = same as $[R_\lambda]_V$ except for the near-infrared region.

The hemispherically integrated upward diffuse fluxes, $I\uparrow$, above the canopy as measured by the sensors would then be given by

$$I\uparrow_V = \int_0^\infty S_\lambda [R_\lambda]_V a_\lambda d\lambda, \tag{35a}$$

$$I\uparrow_N = \int_0^\infty S_\lambda [R_\lambda]_N a_\lambda d\lambda \tag{35b}$$

or

$$I\uparrow_V = \bar{a}_V \int_0^\infty S_\lambda [R_\lambda]_V d\lambda, \tag{36a}$$

$$I\uparrow_N = \bar{a}_N \int_0^\infty S_\lambda [R_\lambda]_N d\lambda, \tag{36b}$$

where the broadband canopy reflectances are given by

$$\bar{a} = \frac{\int_0^\infty S_\lambda [R_\lambda] a_\lambda d\lambda}{\int_0^\infty S_\lambda [R_\lambda] d\lambda}. \tag{37}$$

Combination of (34)–(37) yields

$$\mathrm{SR} = \frac{\bar{a}_N}{\bar{a}_V} = \frac{I\uparrow_N}{I\uparrow_V} \cdot \frac{1}{B}. \tag{38}$$

Since B should be relatively easy to estimate from theory and observations, the combination of radiances in (38) allows one to estimate the simple ratio of the surface reflectances without having to know the values of the incoming radiances. The use of the simple ratio rather than the estimated near-infrared reflectance by itself should therefore provide the observer with some greater certainty about the spectral properties of the surface. In this way, a_V may be used as a kind of standard background to normalize the a_N observations, a practice which would be perfectly justified when ($\rho_s \rightarrow$

$\rho_s')_V$. We may illustrate this point by going back to the example of our photon-throwing experimenter. Provided that he is launching an equal number, or a constant ratio $(1/B)$ of near-infrared and visible photons (i.e., the incoming spectral radiation at the surface), he need not keep count of either as long as he can count the numbers of the photons reflected back. When $(\rho_s \to \rho_s')_V$, the number of reflected visible/PAR photons will be a constant fraction of the number launched regardless of the vegetation density. He thus has a means of quantifying the incident radiation flux density. Since this means that the reflected visible/PAR photons are directly related to the incoming flux density, the ratio of reflected near-infrared to visible photons will be independent of their incoming flux densities and only dependent on the amount of vegetation present.

A second reason for the use of SR, rather than a_N alone, is important in marginal or desert areas where the underlying soil surface is relatively light-colored ($\rho_s > 0.25$). Here the near-infrared signal is not necessarily a sensitive indicator of the presence or absence of vegetation. To take the extreme case, when the soil reflectance in the near-infrared region approaches the asymptotic canopy reflectance, changes in the simple ratio or normalized difference are due solely to variations in the visible reflectance. In this case, we have

$$(\rho_s \to \rho_s')_N, \qquad \frac{\partial a_N}{\partial L_T} \to 0, \quad (39a)$$

$$\frac{\partial(\mathrm{SR})}{\partial L_T}, \; -\frac{\partial a_V}{\partial L_T} \propto e^{-2h_V L_T}. \quad (39b)$$

The relationship between SR and P_c, $1/r_c$, and APAR then becomes curvilinear. For example, taking the case of the relationship between the area-averaged photosynthetic rate P_c and the simple ratio (SR), we then have for a canopy of horizontal leaves

$$\frac{\partial P_c}{\partial(\mathrm{SR})} = \frac{\partial P_c}{\partial L_T} \cdot \frac{\partial L_T}{\partial(\mathrm{SR})} \propto e^{h_V L_T}, \quad (\rho_s \to \rho_s')_N. \quad (40)$$

In this situation, a plot of P_c against SR would show a slow rise in P_c for a large initial increase in SR. With increasing leaf area index, the SR would approach an asymptote, even though the photosynthetic capacity of the surface may be increasing. Although the system is fairly nonlinear under these conditions, it has its greatest sensitivity when the vegetation cover is light, the normal situation in such areas. Clearly, much more information can be extracted from the reflectance data if something is known about the optical properties of the underlying soil.

All of the discussion covered so far in this paper has been concerned with elucidating the biophysical reasons for the apparently near-linear relationship between SR and APAR, P_c, and/or $1/r_c$. However, a number of theoretical limitations in the analysis should be addressed prior to applying these lessons to the practical business of interpreting satellite imagery in a quantitative fashion. These limitations follow the form of the specific assumptions used throughout the analysis. Each of these will be discussed briefly in turn.

i. *Complex leaf angle distributions:* Canopies with more complex leaf angle distribution functions exhibit more complicated responses of SR

with solar angle, unequal leaf reflectance and transmittance values, etc. Similarly, the P_c and $1/r_c$ responses become dependent on solar angle. However, as the paper of Sellers (1985) showed, these effects are not too alarming for reasonable leaf angle distribution functions (i.e., nonerectophile) for high solar elevations.

ii. *Nonisotropic canopy reflectance:* This and the question of satellite sensor narrow-field-of-view radiances cannot be addressed within the constraints of the two-stream approximation model. More sophisticated models (e.g., that of Kimes, 1984) must be used to explore the fine details of narrow angle spectral response versus leaf area index, leaf angle distribution function, etc. Similarly, when canopies have regular or clumped (i.e., nonrandom) leaf distributions, the simple analysis presented here will not translate directly. However, the same principle of near-linearity between SR and APAR, P_c, or $1/r_c$ should still hold as both the process of reflectance and biophysical functioning depend on interactions between radiation and the leaf elements. The effect of nonrandom leaf distributions will be to alter the dependence of SR, APAR, P_c, and $1/r_c$ upon L_T without greatly affecting their interdependence.

iii. *Estimation of mean extinction coefficients:* The calculation of mean scattering and reflectance coefficients [see Eqs. (33) and (37)] via integration over a given wavelength interval is a valid procedure. Application of these mean quantities to estimate equivalent mean extinction coefficients and then to use these in radiative transfer calculations is a different matter. To be exact, such a procedure is mathematically and physically in error but in this particular study of leaf optical properties, where the leaf spectral response is relatively invariant on either side of the 0.68 μm discontinuity, the resultant errors should not be too serious.

iv. *Other environmental factors:* As mentioned elsewhere, even if the condition as stated by (31) were perfectly met in nature (which it is not), then the SR would only provide the functional forms of P_c and $1/r_c$. Additional information, in the form of incident PAR fluxes, leaf physiological properties, and the degree of environmental stress is required in order to determine the actual values of P_c and $1/r_c$.

In spite of the above problems, it is clear that the simple ratio data as provided by satellite remote sensing systems should yield near-linear estimates of the area-averaged canopy photosynthetic capacities and minimum resistances, provided that other quantities are available or can be estimated. This finding supports the view that the reflectance data provide indications of instantaneous rates associated with the vegetation canopies: gross primary productivity and evapotranspiration, rather than reliable estimates of any state associated with the vegetation such as leaf area index or biomass. On a purely practical level, the AVHRR sensor mounted on the NOAA series of polar orbiting meteorological satellites appears to be a near-optimal system for carrying out global biophysical

surveys. Clearly, however, more experimental work needs to be done to determine the quantitative limits to the application of these remote sensing techniques to the measurement of biophysical processes over large areas.

Addendum. The equations in the Appendix of Sellers (1985) contained an error. The expression for h_4 on page 1369 should read:

$$h_4 = -fp_3 - cd.$$

Appendix

Expansion of two-stream approximation expression for hemispherical reflectance

The canopy hemispherical reflectance a is given by the solution to (2) at the limit $L = 0$:

$$a = I\uparrow_{(0)} = h_1/\sigma + h_2 + h_3. \quad (5), (A1)$$

Horizontal leaves. For a canopy of horizontal leaves and with reference to the Appendix of Sellers (1985),

$$h_1 = -\left[\omega\bar{\mu}K\beta_0(b - \bar{\mu}K) + \left(\frac{\omega}{2}\right)^2\right]$$

where

$$b = 1 - \frac{\omega}{2},$$

$$\bar{\mu} = K = 1,$$

$$\beta, \beta_0 = \tfrac{1}{2},$$

and

$$h_1 = -\frac{\omega}{2}\left(-\frac{\omega}{2} + \frac{\omega}{2}\right) = 0,$$

$$h_2 + h_3 = \frac{1}{D_1}\left[\frac{\omega}{2}(u_1 - \bar{\mu}h)\frac{1}{S_1} - \frac{\omega}{2}(u_1 + \bar{\mu}h)S_1\right], \quad (A2)$$

$$D_1 = P_1(u_1 - \bar{\mu}h)\frac{1}{S_1} - P_2(u_1 + \bar{\mu}h)S_1, \quad (A3)$$

where

$$u_1 = 1 - \omega/2 - \omega/2\rho_s$$
$$= 1 - (\omega/2)(1 + 1/\rho_s),$$

$$h = (1-\omega)^{1/2},$$

$$S_1 = e^{-hL_T},$$

$$P_1 = 1 - \omega/2 + h,$$

$$P_2 = 1 - \omega/2 - h.$$

From (A1) and (A2),

$$a = 0 + h_2 + h_3,$$

$$a = \frac{\omega}{2}\left[\frac{(P_2 - \gamma)/S_1 - (P_1 - \gamma)S_1}{P_1(P_2 - \gamma)/S_1 - P_2(P_1 - \gamma)S_1}\right] \quad (A4)$$

where

$$\gamma = \omega/2\rho_s,$$

and

$$a = \frac{\omega}{2}\left(\frac{1 - A}{P_1 - P_2 A}\right),$$

where

$$A = \left(\frac{P_1 - \gamma}{P_2 - \gamma}\right) S_1^2, \qquad S_1 = e^{-hL_T}. \quad \text{(A5)}$$

N.B.: All terms in (A5) depend on scattering properties of vegetation and soil *only* except for S_1 which depends on the value of L_T.

Spherically distributed leaves. Expansion of (5) or (A1) using the substitutions from the Appendix of Sellers (1985) and taking $\bar{\mu} = 1$, $\beta = \frac{1}{2}$, yields

$$\begin{aligned} a = {} & \frac{h_1}{\sigma} + \frac{1}{D_1} \\ & \times \left\{ \left[\omega K \beta_0 - \frac{h_1}{\sigma}\left(1 - \frac{\omega}{2} + k\right)\right] \right. \\ & \quad \times \left[u_1 \left(\frac{1}{S_1} - S_1 \right) - h\left(\frac{1}{S_1} + S_1 \right) \right] \\ & \quad + 2h \left[\omega K \beta_0 - \omega\beta \right. \\ & \quad \left. \left. - \frac{h_1}{\sigma}(u_1 + K) \right] S_2 \right\}, \end{aligned} \quad \text{(A6)}$$

$$\frac{h_1}{\sigma} = \frac{-\omega K}{2} \frac{2\beta_0(1 - \omega - K) + \omega}{K^2 - 1 + \omega},$$

$$\beta_0 = \frac{1 + K}{\omega K} a_{s(\mu)},$$

where

$a_{s(\mu)}$ = single scattering albedo [see Sellers (1985)],

$S_1 = e^{-hL_T}$,

$S_2 = e^{-KL_T}$,

$K = G(\mu)/\mu$,

and

$$D_1 = P_1(u_1 - h)/S_1 - P_2(u_1 + h)S_1.$$

The complete form of (A6) and its derivative used in the study described in the text. The main purpose of the paper, however, was to examine the dependence of the reflectance upon the total leaf area index L_T. For the purpose of illustration we shall consider a simplified version of (A6), which is obtained by assuming

i. $\rho_s \to 0$,
ii. $\beta_0 = \frac{1}{2}$ (actually $\beta_0 = 0.46$ for $\mu = 1$),
iii. $K = \frac{1}{2}$ ($\mu = 1$).

(A6) then reduces to

$$a = \frac{\omega}{2(3 - 4\omega)} \times \left[\frac{(S_1^2 - 1)(1 - 2\omega - h) + 2h(S_1 S_2 - 1)}{(S_1^2 - 1)(1 - \omega/2 - h) - 2h} \right]. \quad \text{(A7)}$$

Calculation of derivative of a with respect to L_T

Horizontal leaves.

$$\begin{aligned} \frac{\partial a}{\partial L_T} &= \frac{\omega}{2} \left[-\frac{\partial A}{\partial L_T} \frac{1}{(P_1 - P_2 A)} \right. \\ &\qquad \left. + \frac{(1 - A)}{(P_1 - P_2 A)^2} P_2 \frac{\partial A}{\partial L_T} \right] \\ &= \frac{\omega}{2} \frac{\partial A}{\partial L_T} \left[\frac{P_2 - P_1}{(P_1 - P_2 A)^2} \right], \end{aligned}$$

where

$$\frac{\partial A}{\partial L_T} = -2hA,$$

and

$$\frac{\partial a}{\partial L_T} = \omega h A \left[\frac{P_1 - P_2}{(P_1 - P_2 A)^2} \right]. \quad \text{(A8)}$$

Spherically distributed leaves. Differentiation of (A7) with respect to L_T yields

$$\frac{\partial a}{\partial L_T} = \frac{2h}{\Delta^2} \Big\{ S_1^2 \Big[(2\omega - 1)(2 - \omega) + \Big(1 - \frac{\omega}{2} + h\Big)(h - K) \times S_1 S_2 - 2h^2 \Big] - \Big(1 - \frac{\omega}{2} - h\Big)(h + K) S_1 S_2 \Big\}, \quad \text{(A9)}$$

where

$$\Delta = (S_1^2 - 1)(1 - \omega/2 + h) - 2h.$$

For the near-infrared case when $\omega_N = 0.95$, the above expression becomes

$$\frac{\partial a}{L_T} = \frac{S_1^2(0.378 - 0.094 S_1 S_2) - 0.098 S_1 S_2}{(0.75 S_1^2 - 1.20)^2}. \quad \text{(A10)}$$

An inspection of the relative size of the terms in (A10) shows that, for reasonable values of L_T,

$$\frac{\partial a}{\partial L_T} \propto S_1^2 = e^{-2h_N L_T},$$

for a first approximation.

χ_L: The Ross–Goudriaan function

Ross (1975) defined a leaf angle distribution function χ_L to describe irregular canopy geometries by means of a single parameter:

$$\chi_L = \pm \int_0^{\pi/2} |1 - O(\theta)| \sin\theta \, d\theta \quad \text{(A11)}$$

where

$O(\theta)$ = leaf angle distribution function,

θ = angle of leaf normal to the local vertical,

χ_L = 0 for spherically leaf angle distributions, + 1 for horizontal leaves and − 1 for vertical leaves.

Goudriaan (1977) fitted a curve to data sets generated from (A11) which provides reasonable estimates of the average leaf projection in any direction as a function of χ_L

$$G(\mu) = \phi_1 + \phi_2 \mu, \quad \text{(A12)}$$

where

$$\phi_1 = 0.5 - 0.633\chi_L - 0.33\chi_L^2,$$
$$\phi_2 = 0.877(1 - 2\phi_1).$$

In Fig. 20, lines are drawn for $\chi_L = -0.5$ (planophile) and $\chi_L = -0.5$ (erectophile) leaf angle distributions. These correspond to average leaf inclination angles of about 19° and 53°, respectively. A spherical leaf angle distribution ($\chi_L = 0$) has an average leaf inclination angle of 30°, horizontal leaves ($\chi_L = 1$) have leaf inclination angles of 0°.

The author is an Assistant Research Scientist working with the Center for Ocean-Land-Atmosphere Interactions (COLAI) at the University of Maryland

and sponsored under NASA Grant NAG 5-492. Useful discussions with A. Dalcher, P. J. Camillo, A. T. C. Chang, C. J. Tucker, D. Strebel, and R. E. Dickinson contributed to some of the ideas in this paper. C. J. Tucker also suggested a number of changes to the text which have been incorporated to improve the clarity of the presentation. J. Norman is to be especially thanked for pointing out the potential suitability of the fifth Thematic Mapper Band (TM-5) in view of Eq. (31). B. N. Holben, S. N. Goward, D. S. Kimes, and B. L. Markham helped with the provision of the relative spectra response curves for the satellite sensors. R. E. Murphy, T. J. Schmugge, and J. Shukla provided encouragement, and Joyce Tippett typed and edited the manuscript.

References

Asrar, G., Fuchs, M., Kanemasu, E. T., and Hatfield, J. L. (1984), Estimating absorbed photosynthetic radiation and leaf area index from spectral reflectance in wheat, *Agron. J.* 76:300–306.

Curran, P. J. (1980), Multispectral photographic remote sensing of vegetation amount and productivity, Proc. 14th Int. Symp. Rem. Sens. Environ., Univ. of Michigan, Ann Arbor, MI, pp. 623–637.

Dickinson, R. E. (1983), Land surface processes and climate-surface albedos and energy balance, *Adv. Geophys.* 25:305–353.

Farquhar, G. D., and von Caemerrer, S. (1982), Modeling of photosynthetic response to environmental conditions, In *Encyclopedia of Plant Physiology, New Series, 12B, Physiological Plant Ecology II* (O. L. Lange et al., Eds.), Springer-Verlag, Berlin ,Heidelberg, pp. 549–587.

Farquhar, G. D., and Sharkey, T. D. (1982), Stomatal conductance and photosynthesis, *Ann. Rev. Plant Physiol.* 33:317–345.

Fung, I. Y., Tucker, C. J., and Prentice, K. C. (1986), On the application of the AVHRR vegetation index to study the atmosphere-biosphere exchange of CO_2, *J. Geophys. Res.*, forthcoming.

Goudriaan, J. (1977), Crop micrometerology: a simulation study, Wageningen Center for Agricultural Publishing and Documentation, Wageningen, Netherlands, 249 pp.

Goward, S. N., Tucker, C. J., and Dye, D. G. (1985), North American vegetation patterns observed with the Nimbus-7 Advanced Very High Resolution Radiometer, *Vegetatio* 64:3–14.

Heimann, M., Keeling, C. D., and Tucker, C. J. (1986), A three-dimensional model of atmospheric CO_2 transport based on observed winds. 2. Analysis of the seasonal cycle of CO_2, *Tellus* (forthcoming).

Kidwell, K. B. (1981), *NOAA Polar Orbiter Data (Tiros-N, NOAA-6 and NOAA-7) Users Guide*, Department of Commerce, Washington, DC, 42 pp.

Kimes, D. S. (1984), Modeling the directional reflectance from complete homogeneous vegetation canopies with various leaf orientation distributions, *J. Opt. Soc. Amer.* 1:725–737.

Kimes, D. S., Sellers, P. J., and Newcomb, W. W. (1986), Hemispherical reflectance (albedo) dynamics of vegetation canopies for global and regional energy budget studies, *J. Clim. Appl. Meteorol.* (forthcoming).

Markham, B. L., and Barker, J. L. (1983), Spectral characterization of the Landsat-4 MSS sensors, *Photogramm. Eng. Remote Sens.* 6:811–833.

Markham, B. L., and Barker, J. L. (1985), Spectral characterization of the Landsat Thematic Mapper sensors, *Int. J. Remote Sens.* 6(5):697–716.

McCree, K. J. (1972), The action spectrum, absorptance and quantum yield of photosynthesis in crop plants, *Agric. Meteorol.* 9:191–216.

Miller, L. D. (1972), *Passive Remote Sensing of Natural Resources*, Dept. of Watershed Science, Colorado State Univ., CO, 1057 pp.

Monteith, J. L. (1977), Climate and the efficiency of crop production in Britain, *Phil. Trans. Roy. Soc. London*, B281:277–294.

Ross, J. (1975), Radiative transfer in plant communities, In *Vegetation and the Atmosphere, 1* (J. L. Monteith, Ed.), Academic, London, pp. 13–52.

Sellers, P. J. (1985), Canopy reflectance, photosynthesis and transpiration, *Int. J. Remote. Sens.* 6(8):1335–1372.

Tucker, C. J., Holben, B. N., Elgin, J. H., and McMurtrey, E. (1981), Remote sensing of total dry matter accumulation in winter wheat, *Remote Sens. Environ.* 11:171–190.